



**Aalto-yliopisto**  
Insinöörیتieteiden  
korkeakoulu

Jani Siniluoto

## **Analysis of impact toughness at the vicinity of the weld fusion line in a S700MC steel**

Espoo 11.12.2019  
Supervisor: Prof Pedro Vilaça  
Advisor: Hamidreza Latifi



---

**Tekijä** Jani Siniluoto

---

**Työn nimi** Iskutuskeyden analysointi hitsin fuusiolinjan läheisyydessä S700MC teräksellä.

---

**Maisteriohjelma** Materiaalitekniikka

**Koodi** ENG 25

---

**Työn valvoja** Pedro Vilaça

---

**Työn ohjaaja(t)** Hamidreza Latifi

---

**Päivämäärä** 11.12.2019

**Sivumäärä** 70

**Kieli** Englanti

---

### Tiivistelmä

Tässä diplomityössä tutkittiin ultralujan teräksen (UHSS) lujuusominaisuuksia hitsin lämpövyöhykkeellä olevalla fuusiolinjalla. Työssä tutkittava teräs oli ultraluja Strenx S700MC Plus.

Kirjallisuussosiossa käsitellään UHSS-terästen hitsattavuutta, lämmön tuottoa ja lämpövyöhykettä sekä lämpövyöhykkeen mikrorakennetta.

Kokeellisessa osiossa saadusta 700MC materiaalista valmistettiin koekappaleet, jotka hitsattiin MIG/MAG-prosessilla Aalto-yliopistolla Espoossa. Hyväksytyille hitsille ja perusaineelle tehtiin rikkovat aineenkoestukset, kuten Charpy (CVN) iskutuskeyskokeet, Vickersin mikrokovuuskokeet sekä vetokoe. Iskutuskeyskokeet suoritettiin hitsin fuusiolinjan näytteille, joita oli yhteensä 51. Alamittaiselle perusmateriaalille tehtiin 30 iskutuskeyskoetta. Rikkomattomia aineenkoestuksia olivat mikroskooppikuvat iskusauvojen sivupinnoista, elektronimikroskooppikuvat (SEM) murtopinnoista sekä perusmateriaalista.

---

**Avainsanat** S700MC, hitsattavuus, lujuus, Charpy, ultra-high strength steel

---



---

**Author** Jani Siniluoto

---

**Title of thesis** Analysis of impact toughness at the vicinity of the weld fusion line in a S700MC steel

---

**Master programme** Mechanical Engineering

**Code** ENG 25

---

**Thesis supervisor** Pedro Vilaça

---

**Thesis advisor(s)** Hamidreza Latifi

---

**Date** 11.12.2019

**Number of pages** 70

**Language** English

---

### **Abstract**

The objective for this master's thesis was research ultra-high strength steel (UHSS) and characterization of impact toughness and microstructure properties at the vicinity of the fusion line and HAZ. The welding process used was conventional MIG/MAG-welding and the material was Strenx S700MC Plus.

In the literature part, weldability, heat input, heat-affected zones, sub-zones and microstructure are discussed.

Experimental part of the study weld was investigated with several mechanical tests and optical tests. Non-destructive tests used, where for example light optical microstructural pictures and scanning electron microscopy pictures were taken. Destructive tests for example Vickers microhardness, tensile and total 51 Charpy-V impact tests were carried out. Side-profiles of samples were pictured. Base material was also tested with 30 sub-sized samples.

---

**Keywords** S700MC, weldability, toughness, Charpy, ultra-high strength steel

---



## Foreword

I want to express my gratitude to Aalto University's Mechanical Engineering Advanced Materials (AM2) research group for their support. Big thanks to the technical staff at K2-building, without them this work would not have been carried out successfully. I want to thank especially Laura Tiainen, Seppo Nurmi and Kim Widell for your effort to this work. Thanks to Patrik Sahiluoma for helping with my SEM-pictures and big thanks to the Virpi Ojala and Helena Suonsilta at K1 building. Big thanks go to my wife Nina, for her support.

My thesis advisor, MSc, PhD student Hamidreza Latifi, was important for my thesis and big thanks for your effort to this study. Also, I would like to thank thesis supervisor Prof. Pedro Vilaça for his support and opportunity for this work. This literally was last opportunity for me.

Espoo 11.12.2019

Jani Siniluoto

## Table of contents

Foreword .....	iii
Symbols .....	vi
Abbreviations .....	vii
1 Introduction .....	1
1.1 Scope of the thesis .....	1
1.2 Workplan and objectives .....	2
1.3 Structure of the thesis .....	2
2 Literature review .....	4
2.1 MIG/MAG welding.....	4
2.2 Ultra-high strength steels (UHSS) .....	6
2.2.1 Weldability of UHSS .....	6
2.2.2 Heat input .....	8
2.2.3 Heat affected zone (HAZ).....	9
2.2.4 Sub-zones in HAZ.....	10
2.2.5 Toughness and hardness of UHSS .....	12
2.3 Mechanisms of fracture surface .....	13
3 Experimental conditions and procedures .....	14
3.1 Base material .....	14
3.2 Welding methods and conditions .....	14
3.2.1 Welding equipment .....	14
3.2.2 Clamping .....	15
3.2.3 Consumables .....	16
3.2.4 Joint design .....	16
3.2.5 Welding parameters .....	16
3.3 Testing methods .....	17
3.3.1 Optical microscopy .....	17
3.3.2 Scanning electron microscopy .....	18
3.3.3 Microhardness .....	18
3.3.4 Tensile test .....	19
3.3.5 Charpy's impact test (CVN) .....	20
3.4 Extraction plan for samples .....	23
4 Base material results .....	24
4.1 Optical microscopy.....	24
4.2 Microhardness .....	25
4.3 Toughness.....	26
5 Weld joints results.....	27
5.1 Optical microscopy.....	27
5.1.1 Macrograph .....	27
5.1.2 Micrograph.....	27
5.2 Scanning electron microscopy (SEM).....	28
5.3 Microhardness .....	30
5.4 Tensile strength .....	32
5.5 Charpy's impact test (CVN).....	32
5.6 Fractography.....	37
6 Conclusions .....	38
7 List of references.....	39

APPENDIX 1: WELDING PROCEDURE SPECIFICATION (WPS SFS EN ISO 15609-1:2004)

APPENDIX 2: SAMPLE LOCATIONS (SFS EN-ISO 15614-1:2017)

APPENDIX 3: CVN RESULTS (SAMPLES 1-51)

APPENDIX 4: CVN FRACTURE SURFACES

APPENDIX 5: SEM PICTURES

APPENDIX 6: CVN IMPACT TOUGHNESS SIDE PROFILE PICTURES OF THE SUB-SIZED BASE MATERIAL (15 + 15 SAMPLES)

APPENDIX 7: CVN IMPACT TOUGHNESS SIDE PROFILE PICTURES FROM THE WELD (51 SAMPLES)

APPENDIX 8: TENSILE TEST GRAPH

APPENDIX 9: PICTURE OF THE WELD

## Symbols

$A_0$	Area of the tensile test specimen
BM	Base Material
CE	Carbon Equivalent
E	Arc energy
$F_2$	2-dimensional heat flow
$F_3$	3-dimensional heat flow
I	Current [I]
k	Ratio of heat efficiency
kN	kiloNewton
MPa	Megapascal, (N/mm <sup>2</sup> )
$R_m$	Tensile strength
$R_{p0,2}$	0,2- limit
$\Delta t_{8/5}$	Time from 800°C to 500°C
U	Arc voltage [U]
v	Welding speed (mm/s)
Q	Heat input (kJ/mm)
$\varepsilon_{eng}$	Strain (engineer)
$\sigma_{eng}$	Stress (engineer)

## Abbreviations

AHHS	Advanced High Strength Steel
BM	Base Material
CCT	Continuous Cooling Time
CEN	Carbon Equivalent Number
CEV	Carbon Equivalent Value
CGHAZ	Coarse Grain Heat-Affected Zone
CVN	Charpy V-Notch
FGHAZ	Fine Grained Heat Affected Zone
FL	Fusion Line
FZ	Fusion Zone
GMAW	Gas Metal Arc Welding
HAZ	Heat Affected Zone
HSS	High Strength Steel
HV	Vickers Hardness
ICHAZ	Intercritically Heat Affected Zone
MAG	Metal Arc Welding
MIG	Metal Inert Gas Welding
NDT/DT	Non-Destructive test/Destructive test
ND	Normal to Rolling Direction
PMZ	Partially Melted Zone
RD	Rolling Direction
SCHAZ	Subcritical Heat Affected Zone
SEM	Scanning Electron Microscopy
TD	Transverse Direction
TMCP	Thermomechanically Controlled Process
TS	Tensile Strength
UHSS	Ultra High Strength Steel
UTS	Ultimate Tensile Strength
WM	Weld Material
WPS	Welding Procedure Specification
YS	Yield Strength



# 1 Introduction

Ultra-high strength steels (UHSS) are modern high strength steels (HSS) with an excellent combination of toughness and strength. The definition for UHSS is still pending on due universal harmonization and different classifications can be found from different authors. UHSS are widely used and welding is the most important manufacturing process in construction and manufacturing industry. Most of the applications for UHSS are in the field of transportation, mining and shipbuilding industry. [1, 2]

In recent years, there has been an increasing interest to utilize UHSS with tensile stress higher than 700 MPa and yield strength over 560 MPa. Recent articles suggest the upper limit of yield strength for commercial grades of UHSS has reached 1400 MPa. Automotive industry is using HSS, typically addressed as advanced high strength steels (AHSS – denomination for sheet metal) to increase safety in collision, and shipbuilding industry uses the UHSS (denomination for plates) it for lighter and stronger structures in ships. Lighter but stronger structure is one way to save energy, transport and manufacturing related costs in the future. This is also a way to minimize the carbon footprint and improve the energy efficiency via lower fuel consumption. Figure 1 shows potential weight save and a percentage when using Strenx structural steels compared to regular structural steel. [2, 3]

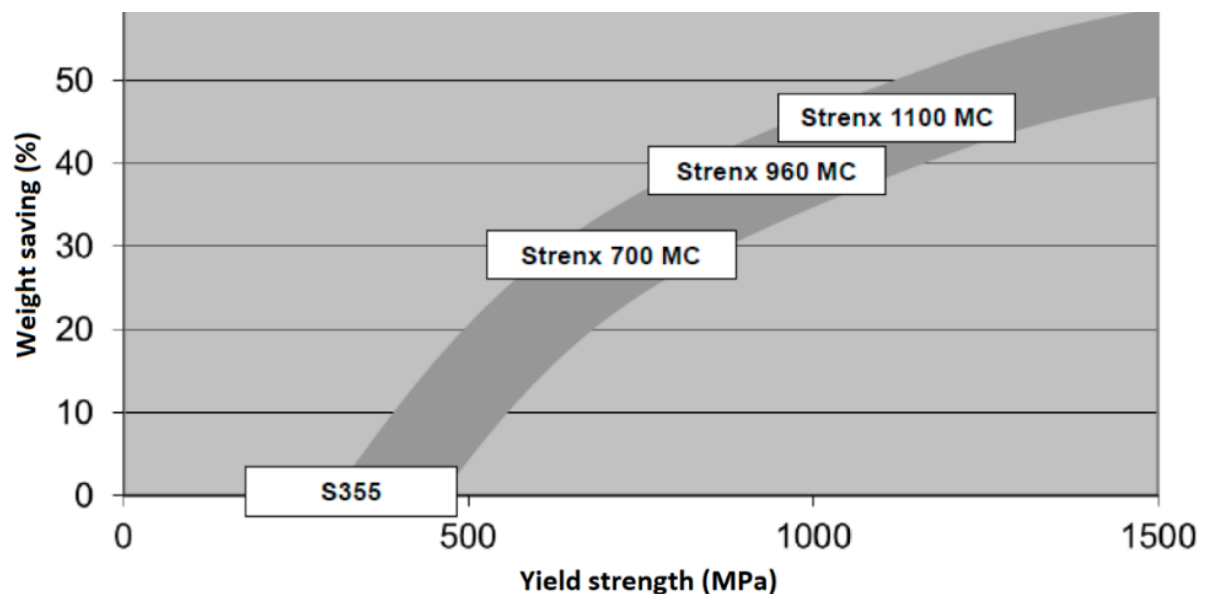


Figure 1. Weight saving (%) compared to regular structural steel S355. [3]

## 1.1 Scope of the thesis

Weldability is an important property for UHSS. Although the UHSS can be successfully welded by gas metal arc welding (GMAW or equivalently denominated by metal inert/active gas welding MIG/MAG), keeping the good original combination of toughness and strength is challenging, mostly at the vicinity of the fusion line. Also, high heat input (Q) can destroy the original good mechanical properties obtained in the UHSS via thermomechanically controlled processing (TMCP). [2]

This study focused on mechanical properties of the base material and weld zone. The properties assessed for the base material will be used as a comparative value to establish the weldability of the UHSS. The weld zone encompasses the fusion zone (FZ), fusion line (FL) and heat affected zone (HAZ). In reality, the FL is not a line, but it contains a thin thickness of partially melted zone, between the FZ and HAZ. The low toughness of the FL in UHSS is typically the major source of the limited weldability of the UHSS.

The main purpose of the study at Aalto was to provide fundamental information on the toughness at the vicinity of the FL in UHSS, when conventional welding procedure specification (WPS) are implemented. The mechanical properties of the base material and the welds produced with conventional WPS will serve in later stages of the ongoing research at Aalto, to compare with the mechanical performance resulting from advanced and specially tailored WPS for MIG/MAG welding of UHSS. The conventional WPS implemented in this study is similar to the one tested in Teemu Lahtinen's Master Thesis (2016) "Analysis and development of weldability of Novel 700 MPa high strength steels". But in Teemu's work, the welds have been done with an automatized system at welding laboratory of SSAB (Raahe) and in this research, the welds are done with a robotized system at the welding laboratory of Aalto.

## 1.2 Workplan and objectives

The workplan is based on the investigation of the mechanical properties and microstructural analysis of the S700MC base material and weld zone, with focus on the toughness at the fusion line. The objectives are:

- To assess the microstructure of main directions of base material and weld joints. Optical microscopy was done for both base material and weld joints and SEM was additionally done for the welded specimens;
- To evaluate the microhardness (HV1) in the main directions of base material and in cross section of the weld joints;
- To measure the toughness (via Charpy's impact test) of base material and weld joints in similar reduced specimen size. The notch in welded specimens is located in multiple zones of the fusion zone, with focus on the vicinity of the fusion line;
- To implement a fractography analysis of the specimens from toughness tests. The fractography was done with SEM of fracture surfaces and side profile analysis of the crack propagation;
- To evaluate the tensile strength of the welded joints.

## 1.3 Structure of the thesis

After introduction, chapter 2 consists of a literature review, which includes MIG/MAG welding process, characterization of UHSS, weldability, heat-input, HAZ and sub-zones in HAZ. Toughness of UHSS and surface fracture mechanisms are also part of the literature review. Experimental conditions and procedures include information about welding equipment's, clamping, consumables, joint design and parameters. Testing methods describes the theory and methods behind the mechanical procedures used in this study. Extraction plan for samples is last part of testing method chapter. Chapter 4 contains base material characterization and includes base material toughness,



microhardness and microstructure results. Results from the welds are presented in chapter 5 and conclusions are compiled in the chapter 6. Side profile pictures from all Charpy impact toughness samples were photographed and pictures are collected in annex.

## 2 Literature review

### 2.1 MIG/MAG welding

Gas metal arc welding (GMAW) is one of most important and commonly used joining processes in manufacturing industry. GMAW is a weld process for melting and joining metals and process uses continuously feed of metal wire and shielding gas. The GMAW process is defined by shielding gas used. Metal active gas welding (MAG) is welding with active gas and usually this is a mixture of 75% carbon dioxide ( $\text{CO}_2$ ) and 25% oxygen ( $\text{O}_2$ ). Active gas is generally used for ferrous materials. [4] Metal-inert gas welding (MIG) is welding with an inert gas which protects molten metal from oxygen and nitrogen ( $\text{N}_2$ ) in the air. In MIG-welding commonly used inert gases are argon (Ar) and helium (He). MIG-welding is the most widely used arc welding process for non-ferrous materials like aluminum alloys. Consumables have a significant effect on the properties and the results. Overall process presented in figure 2. [4, 5]

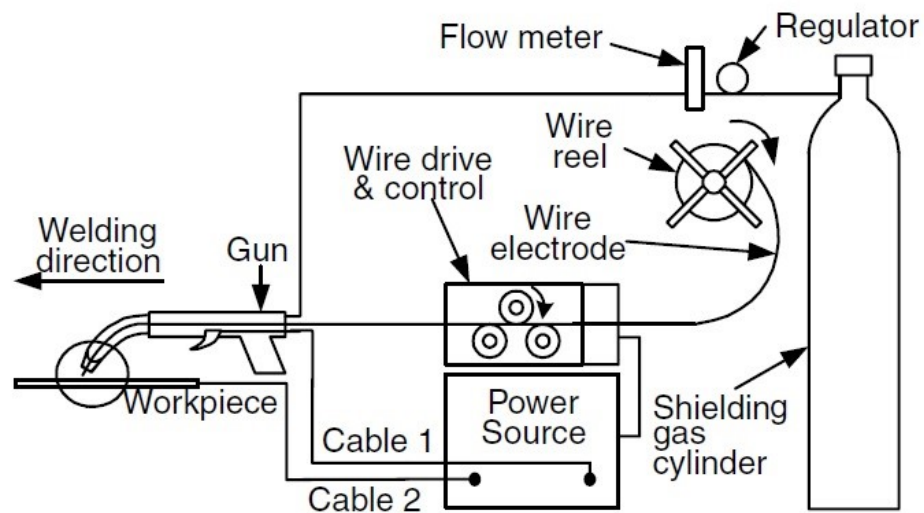


Figure 2. Overall process. [4]

According to the standard SFS EN-ISO 4063 MIG/MAG welding processes have International Institute of Welding (IIW) process numbers, 131 and 135. Process number 131 is for MIG welding and 135 is for MAG welding. SFS EN-ISO 4063 Standard defines process 135 as “MAG welding with solid wire electrode, GMAW using active gas with solid wire electrode”. GMAW is using direct-current electrode positive (DCEP) and filler wire works like electrode. With direct-current electrode negative (DCEN) or alternative current (AC) metal transfer is erratic. Shielding gas is brought through a gas nozzle, as shown in figure 3. [5, 6]

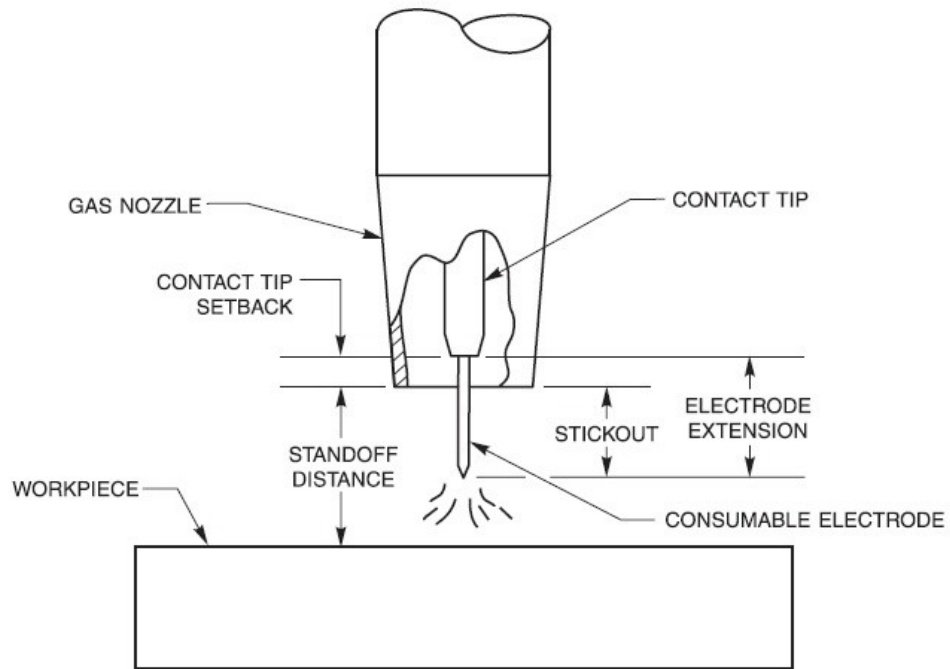


Figure 3. MIG/MAG fusion welding process. [7]

The most common metal transfer in GMAW is spray arc. In this method small metal drops travel across the arc gap under the influence of the electromagnetic force at much higher frequency and speed than in the globular mode. [4]

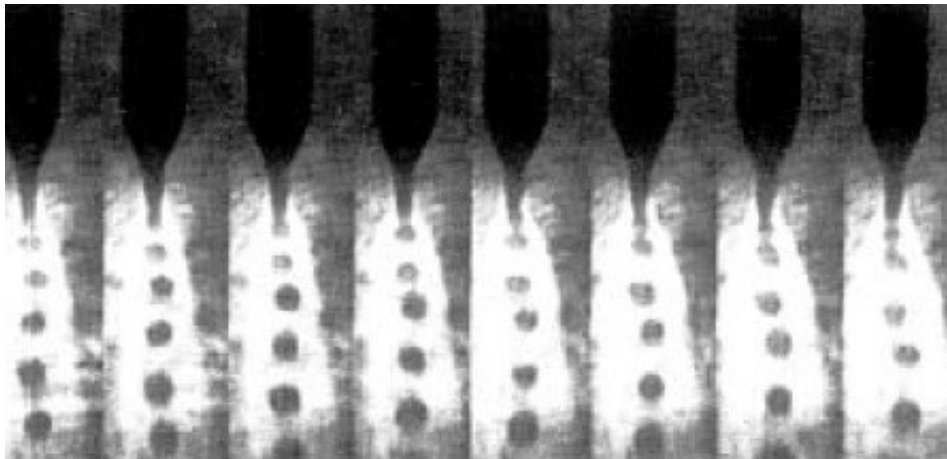


Figure 4. Spray transfer at 320A and 29V. [4]

## 2.2 Ultra-high strength steels (UHSS)

UHSS are also known as high-strength low-alloy steels. TMCP is a controlled rolling (CR) and cooling technique. The CR stage is used to refine the grains and strain the austenite. TMCP control is used to obtain excellent mechanical properties for steel plates such as weldability, strength and toughness. TMCP includes three stages, hot rolling, (HR) quenching and tempering, (Q+T) and high tempering temperature, (HTT) as shown in figure 5. The aim of the Q+T phase is to produce a mixed microstructure consisting of martensite or mixture of bainite and martensite. This complicated microstructure is achieved by rapidly cooling the material sufficiently from the austenite phase. This will avoid the formation of softer phases such as ferrite. [8, 9]

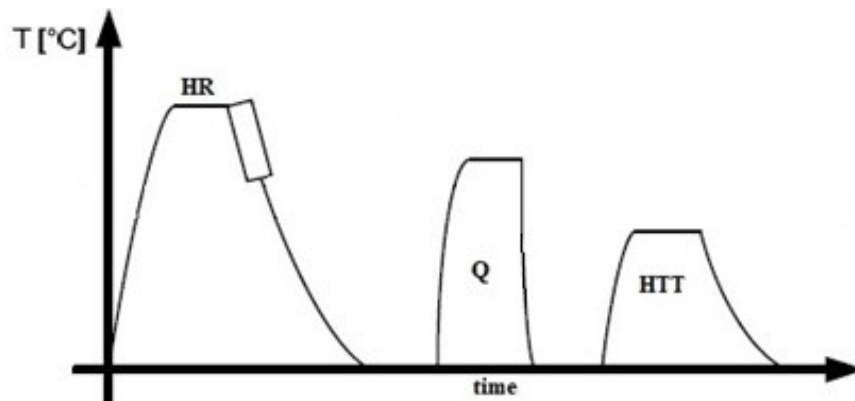


Figure 5. Modified TMCP production process. [8]

TMCP technique helps control microstructure and TMCP can also reduce alloying and improve weldability. Chemical composition, ladle analysis and mechanical properties are determined in SFS EN-ISO 10149-2 as '*Hot-rolled flat products, Technical delivery conditions for thermo mechanically rolled steels*'. Most common micro-alloying elements are Vanadium, (V), Niobium, (Nb) and Titanium (Ti). Micro-alloying elements can preserve a fine grain microstructure and sum of these three elements shall be max 0,22 %. [9, 10]

### 2.2.1 Weldability of UHSS

Metallurgical processes in steel are heating and cooling dependent. The welding thermal cycle in TMCP plays a key role in the evolution of fine grain microstructure and weldability as presented in figure 6. [11]

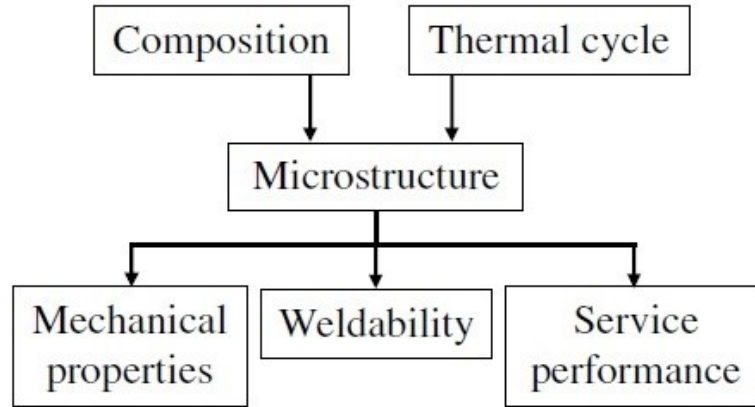


Figure 6. Figure shows weld microstructure evolution and performance in welding. [11]

Weldability is defined by carbon content. The carbon content of UHSS controls strength and hardness at Q+T stage. Most common carbon equivalent formula (CEV) for weldability is, International Institute for Welding (IIW) formula which is presented in equation 1. Usually CEV is in the range 0,30 to 0,40 and material does not need pre-heating. [12, 13]

$$CEV = C + \frac{Mn}{6} + \frac{Cr + Mo + V}{5} + \frac{Ni + Cu}{15} \quad (1)$$

Carbon equivalent (CET) formula is suitable for Q + T steels and cold cracking behavior. CET equation provides information on the effect on the individual alloying elements compared to carbon. An increase of alloy content, plate thickness and hydrogen (H<sub>2</sub>) content increases the risk of cold cracking in steel, notably hydrogen induced cracking (HIC). Formula for CET is presented in equation 2. [12]

$$CET = C + \frac{Mn+Mo}{10} + \frac{Cr+Cu}{20} + \frac{Ni}{40} \quad (2)$$

Third important carbon equivalent formula for weldability was developed 1968 in Japan (Ito – Bessyo) and this equation is based on a wider range of low alloy steels. [14]

$$P_{CM} = \frac{Si}{30} + \frac{Mn}{20} + \frac{Cu}{20} + \frac{Ni}{60} + \frac{Cr}{20} + \frac{Mo}{15} + \frac{V}{10} + 5B \quad (3)$$

According to SFS EN-ISO 1011-2 the  $t_{8/5}$  cooling time (from 800 °C to 500 °C) can be derived from two-dimensional and three-dimensional heat flow equations. Equation for two-dimensional heat flow is presented in equation 4, equation for three-dimensional heat flow is presented in equation 5. Cooling time  $t_{8/5}$  is also known as “continuous cooling time “(CCT). CCT diagrams are important for achieved microstructure changes. [14]

$$t/5 = (4300 - 4.3 \times T_0) \times 10^5 \times \frac{k^2 E^2}{d^2} \times \left[ \left( \frac{1}{500 - T_0} \right)^2 - \left( \frac{1}{800 - T_0} \right)^2 \right] \times F_2 \quad (4)$$

$$t/5 = (6700 - 5 \times T_0) \times k \times E \times \left[ \left( \frac{1}{500 - T_0} \right)^2 - \left( \frac{1}{800 - T_0} \right)^2 \right] \times F_3 \quad (5)$$

$F_2$  = Shape factor for two-dimensional heat flow and for thin plate

$F_3$  = Shape factor for three-dimensional heat flow and for thick plate.

Figure 7 shows two-dimensional and three-dimensional heat flows. Two-dimensional is more suitable for thin plates and three-dimensional for thick plates. [12]



Figure 7. Two and three-dimensional heat flows. Modified. [12]

### 2.2.2 Heat input

“The heat input shall be chosen to be matched to the welding process. For many steels, abrupt cooling from the heat of welding is to be avoided, can be exposed to thermal energy, because of the risk of hardening or cracking” according to SFS EN-ISO 1011-1. Heat input (Q) is relationship between current (I) and voltage (U). These influences the time and temperature cycle occurring during welding. Formula for the heat input and arc energy (E) is shown in equation 6. [4, 15]

$$E = \frac{60 \times U \times I}{1000 \times v} \quad (6)$$

$k$  = thermal efficiency factor, for MIG/MAG this factor is 0,8.

Q = heat input, (kJ/mm)

$Q = k \times E$

U = arc voltage, [V]

I = welding current, [A]

$v$  = travel speed in mm/s

There are several advantages of increasing the power density of the heat source. Weld penetration is deeper and welding speed is higher. Weld quality is better, and workpiece is less damaged. Power density versus high heat is show in figure 8. There are also disadvantages of higher Q. High Q is problematic during welding and will most likely dissolve the carbide and nitride particles and make them lose their effectiveness as grain growth inhibitors. Higher Q can also cause internal stresses and these stresses can lead to cracking in the weld deposit and HAZ. [4, 15]

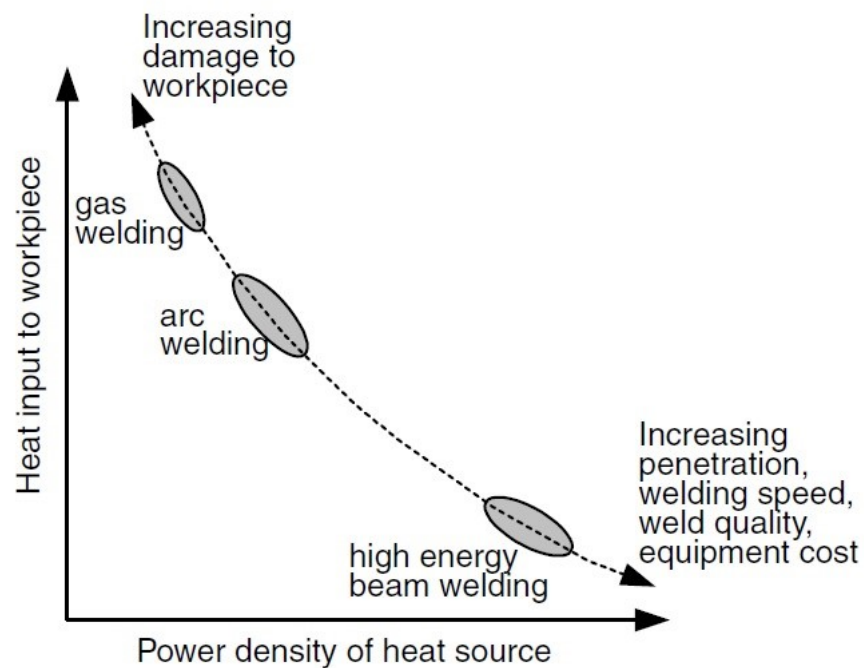


Figure 8. Heat input versus power density. [4]

### 2.2.3 Heat affected zone (HAZ)

The heat-affected zone (HAZ) is the portion of the material, which has not been melted, and because of this, the dilution of weld material can vary in the HAZ. Dilution is the amount of the parent metal/base material that is melted and participates in the constitution of the welding metal. In many cases HAZ is the most critical part of a weld. Softening is caused by coarsening in HAZ due to high heat input,  $Q$  [16, 17]. Microstructure (grain size) and mechanical properties are altered by the heat input and cooling time. [18] A welded joint has three important zones and these zones are presented in figure 9. First zone is the HAZ, second is the partially melted zone (PMZ) and the third one is the fusion zone (FZ). Two important parameters in a HAZ are peak temperature ( $T_p$ ) and already introduced cooling rate  $t_{8/5}$ . [11, 19]

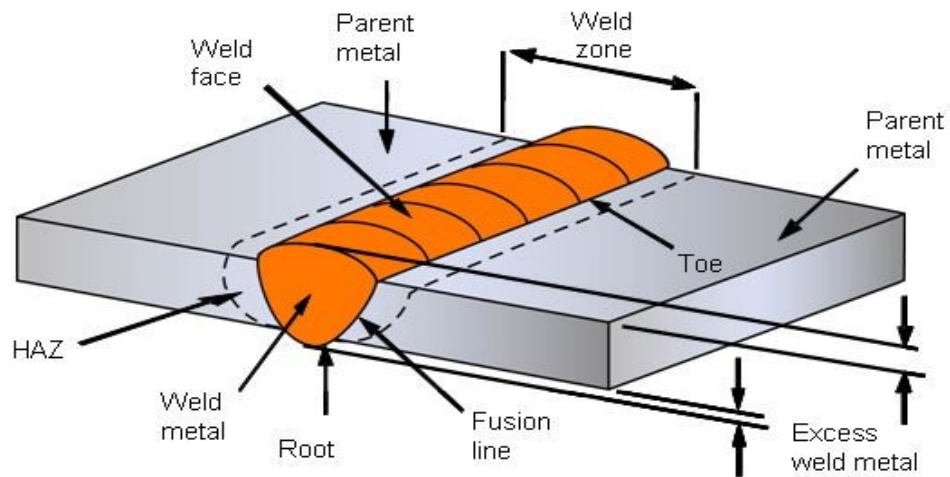


Figure 9. Weld, HAZ and base material. [20]

There can be many possible metallurgical reactions in a weld and HAZ, all areas in the HAZ can undergo one or more of the following reactions. [11]

1. Recrystallization
2. Grain growth
3. Phase transformations
4. Dissolution/overaging of precipitates
5. Precipitate formation
6. Residual stress and stress relaxation

#### 2.2.4 Sub-zones in HAZ

HAZ can be divided into several sub-zones. Due to the softening and other metallurgical effects, the areas around the fusion line may be weaker than the adjacent metal.  $T_p$  is presented on the horizontal line and the vertical line describes the carbon in steel (0,15%). HAZ sub-zones are presented in figure 10. [21]



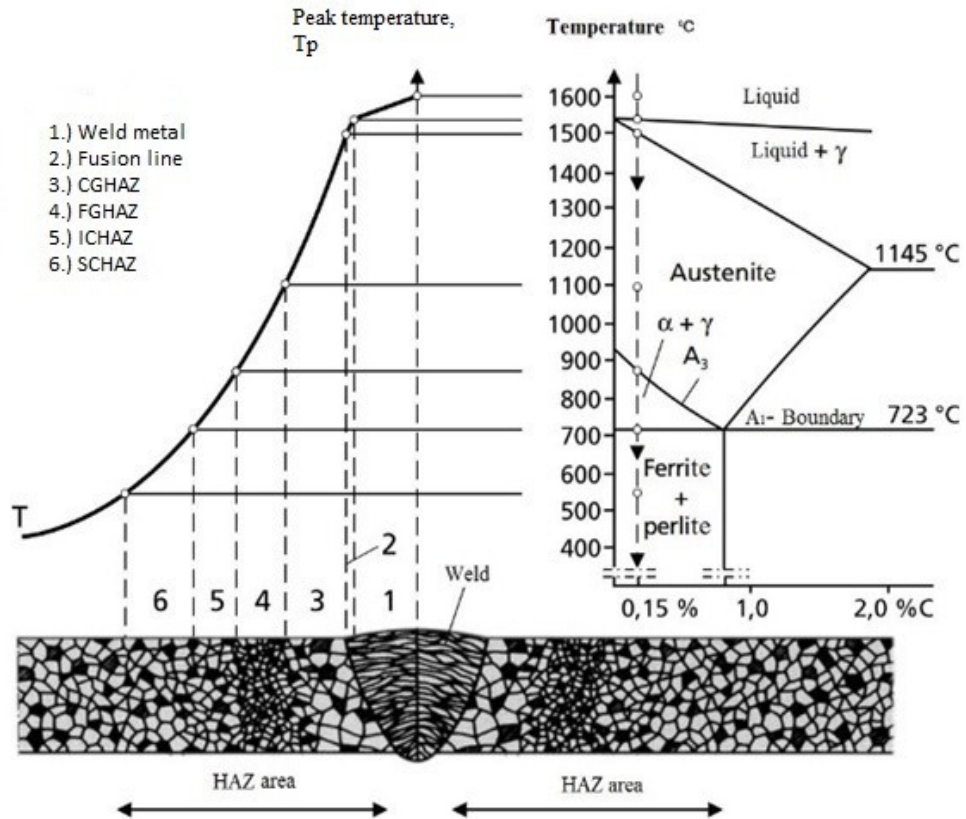


Figure 10. Rautaruukki Oy, heat input and sub-zones. – Modified. [22]

- 1) Weld metal (WM)
- 2) Fusion line, partially melted zone (PMZ)
- 3) Coarse-grained zone (CGHAZ)
- 4) Fine-grained zone (FGHAZ)
- 5) Partially austenitized and tempered zone (ICHAZ)
- 6) Tempered zone (SCHAZ).

First two sub-zones in the HAZ are:

1. WM is a chemical composition and mixture of BM and filler metal. Toughness can be reduced during reheating, multipass welds and microalloying elements such as Nb, Ti, V. [22]
2. Base material fusion line. Usual value for base material dilution is in the range of 20 to 40% for the most frequent joint processes and often this boundary line is called PMZ. [18]

The rest four sub-zones in the HAZ are CGHAZ (3) adjacent to the fusion line, the FGHAZ (4), the zone of ICHAZ (5) and the zone of SCHAZ (6). These zones are presented in figure 11. [23]

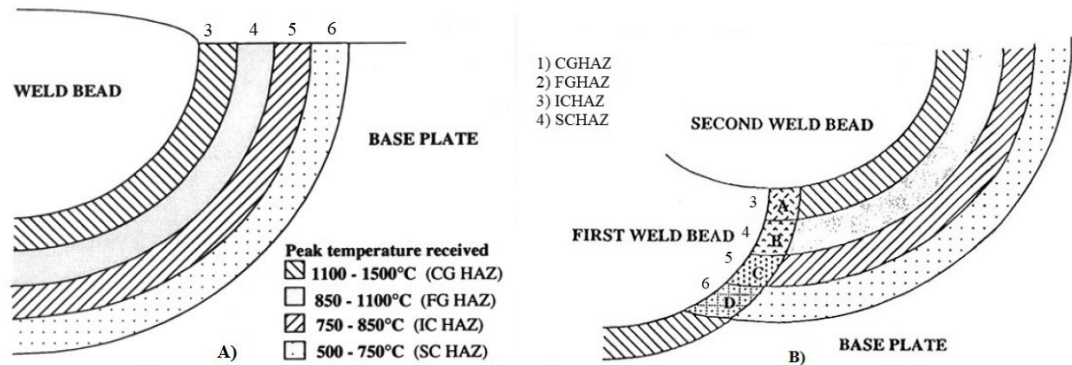


Figure 11. HAZ sub-zones. a) Single pass weld, b) multipass weld. [23]

All four sub-zones are described below.

- 1.) CGHAZ is adjacent to FL.  $T_p$  temperature range is from 1100°C to 1500°C. CGHAZ and coarse-grained weld deposits have therefore a higher hardenability. This area is partially melted, and much bigger grain size makes it weakest point of weld. Impact toughness of the weld is poorest in the CGHAZ area due to brittle and hard phases which have formed as the consequence of fast cooling rate. [21, 24]
- 2.) FGHAZ region is adjacent to the CGHAZ and is comprised of fine-grained ferrite and tempered bainite. Temperature range has been over  $A_3$ -temperature (850 – 1100°C). FGHAZ area has better mechanical properties than PMZ. Microstructure is fine-grained ferrite or fine-grained pearlite. FGHAZ has good impact toughness and hardness. [21, 25]
- 3.) ICHAZ area is partially reheated and temperature range has been middle of  $A_1$  and  $A_3$  (750°C – 850°C). Austenite and ferrite regions contain isolate or tempered martensite – austenite blocks and in low-carbon TMCP steels impact toughness at ICHAZ is generally low. [24, 26]
- 4.) In SCHAZ area, peak temperature range ( $T_p$ ) is 600°C – 700°C. Temperature has been under  $A_1$ - limit temperature (austenite region) and the microstructure hasn't changed. Impact toughness is lower, and this region is mostly tempered martensite with bainite. [25, 26]

### 2.2.5 Toughness and hardness of UHSS

Most important mechanical properties of UHSS are strength, ductility, and stiffness and toughness. Usually toughness is assessed by using an impact test. In HAZ fracture toughness can vary considerably over relatively short distances. [27, 28] According to standard SFS EN-ISO 10149-1 the minimum impact energy value at -20 °C will be 40 J or more and the minimum impact energy value at -40 °C will be 27 J or more. Many studies have lately shown that at -60 °C temperature impact energy goes under 20 J. [10, 29]

Hardness is defined “as the resistance of a material”. High hardness is often described with brittle behavior and microhardness test can help identify low toughness regions in metals. In a recent study, “Influence of welding on dynamic fracture toughness of Strenx 700MC steel” it is shown that Vickers microhardness (HV1) values can vary from 200 to 300 in weld HAZ. [28, 31]

### 2.3 Mechanisms of fracture surface

The most common fracture mechanisms in metals are ductile, cleavage (also often called brittle fracture), intergranular fracture and fatigue. This study does not cover fatigue. Three most common fracture mechanisms are presented in figure 12. [28]

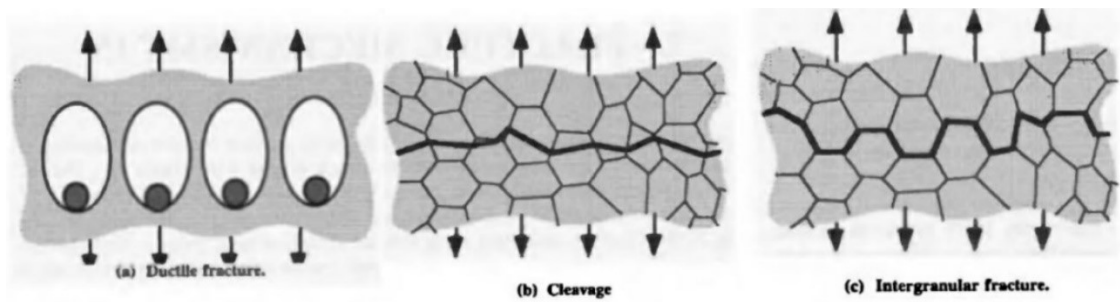


Figure 12. Three fracture micromechanisms, a) ductile, b) cleavage and c) intergranular. [28]

Ductile fracture is often described by nucleation of microvoids and cup-like dimples. After the fracture different size of microvoids and dimples are found on the fracture surface. Pictures of microvoids and dimples on the fracture surface are presented in figure 13. [30]

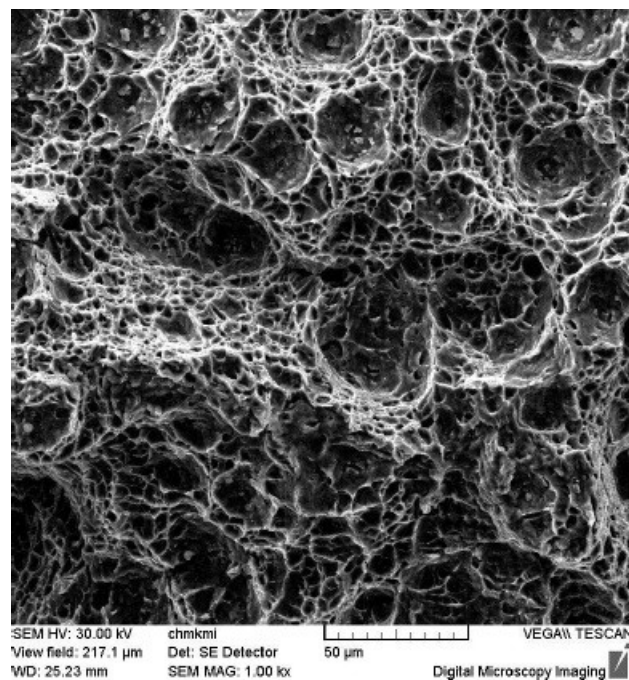


Figure 13. Microvoids and dimples on ductile fracture surface. [30]

According to the literature, there is no single mechanism for intergranular fracture. Intergranular fracture is also often called intercrystalline fracture. The intergranular fracture usually occurs when the grain boundaries are on the fracture path in the material or phases are located on the grain boundary. [32] Brittle fracture may not always be cleavage mode of fracture, but brittle fracture can also occur without cleavage. A fracture is said to be brittle in metals, if the impact energy is low or the plasticity at the crack tip is limited. Usually the crack path of cleavage is river-like. [28, 32]

### 3 Experimental conditions and procedures

#### 3.1 Base material

Base material (BM) of bainitic-ferritic microstructure used in this study was UHSS S700MC plus and material thickness was 8 mm. According to the steel designations system standard SFS EN-10027-1:2016 S700MC plus is structural steel (S), thermo mechanically rolled (M) and cold formed (C) fine grain steel with high yield strength 700 MPa. Table 1 represents the chemical composition of the S700MC and mechanical properties of the S700MC are presented in table 2. [33]

*Table 1. Chemical composition (ladle analysis) of S700MC Plus. Max weight % of the elements (except Al). [34]*

C	Si	Mn	P	S	Al (min)	Nb	V	Ti
0.12	0.21	2.10	0.020	0.010	0.015	0.09	0.020	0.015

*Table 2. Mechanical properties of the S700 MC Plus. [34]*

Steel grade	Thickness (mm)	Minimum yield strength (MPa)	Minimum Elongation $A_5$ (%)	Tensile strength, $R_m$ (MPa)	Min. inner bending radius for a 90° bend
S700MC	3 - 10	700	13	750 - 950	1.0 x t

#### 3.2 Welding methods and conditions

##### 3.2.1 Welding equipment

Runs were carried out by KUKA, KR 5-2 HW mechanical welding robot as seen in figure 14 a) and Fronius VR 7000 Cold Metal Transfer (CMT) control unit as seen in figure 14 b). During welding the arm was equipped with a camera for video recording. In this study Fronius CMT control was not used, instead spray arc mode was used. [35]



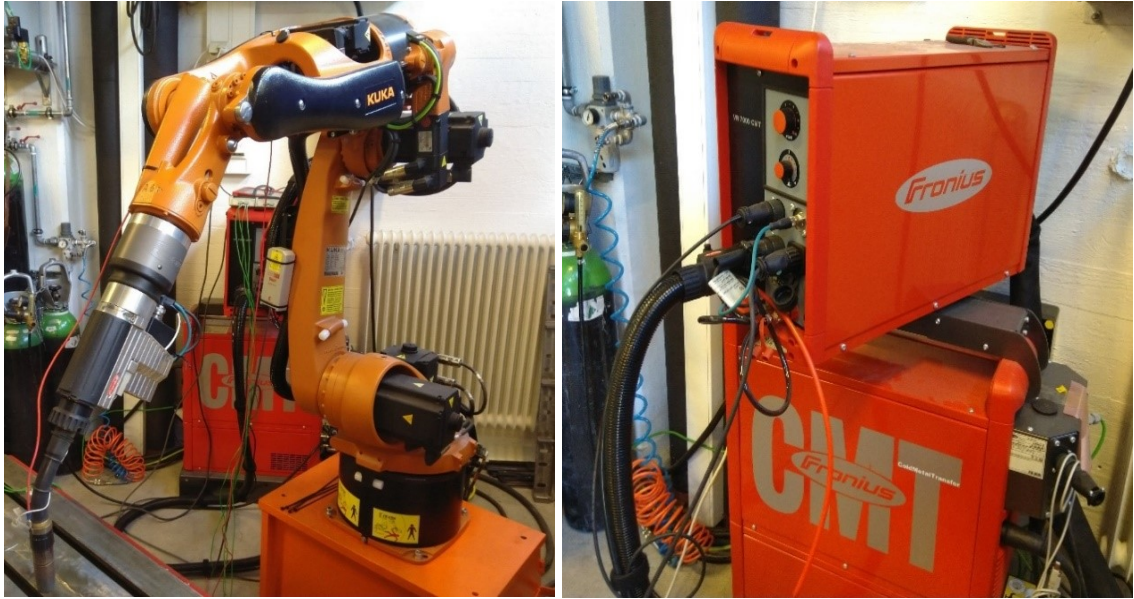


*Figure 14 a) KUKA KR 5-2 HW welding robot and 14 b) Fronius VR 7000 CMT control unit.*

### 3.2.2 Clamping

Support bars and steel plates were clamped on the welding table. Clamping is needed because heat could distort plates. Angular misalignment could cause problems later when milling samples for the Charpy and tensile tests. Clamps and support bars are presented in figure 15.

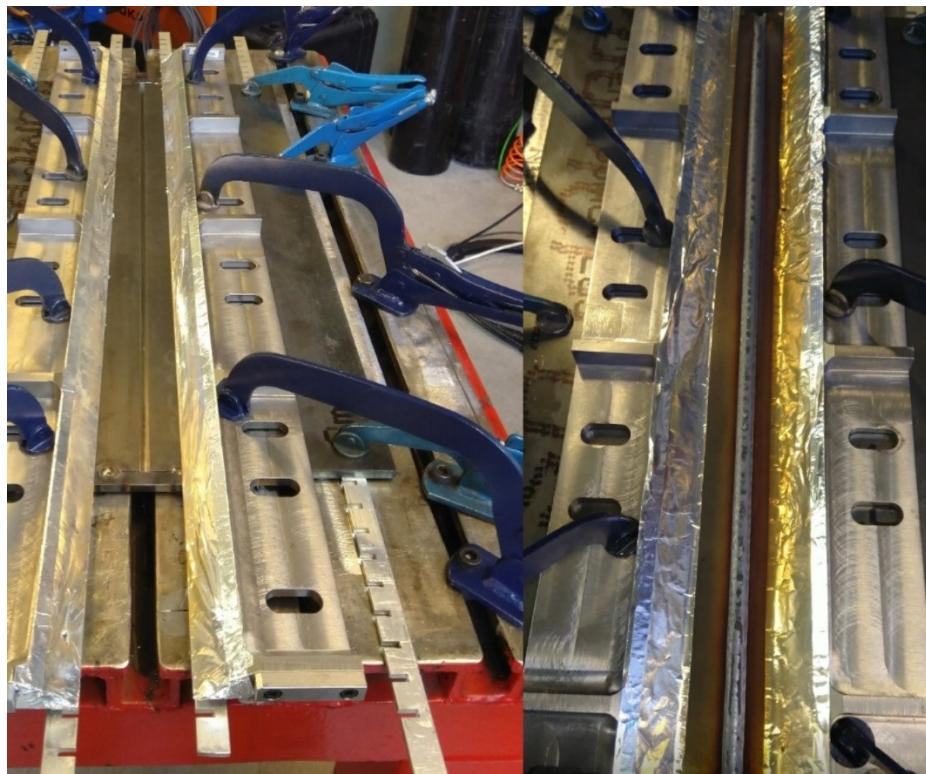


*Figure 15. Support bars and clamps.*

### 3.2.3 Consumables

In this study S700MC was welded using a Böhler X70-IG and wire used was a copper coated solid wire. The Wire is designed for high strength, quenched and tempered fine grain constructional steel and is suitable for HSS with minimum yield strength of 690 MPa. Böhler X70-IG wire also has good impact strength in low temperatures down to -50° Celsius. [36]

The shielding gas used was Mison 8 (M20). According to the gas manufacturer AGA, gas is suitable for low alloy steels, robotic and mechanized welding. The gas is designed for spray arc and pulse welding. Mison 8 shielding gas contains 8 % CO<sub>2</sub> and 0,03 % nitric oxide (NO). [37, 38]

### 3.2.4 Joint design

Dimensions for the welding plates were 8 × 200 × 1000 mm. There was no air-gap or root surface between plates, the angle for V-groove butt weld was 50°. Joint design is presented in figure 16.

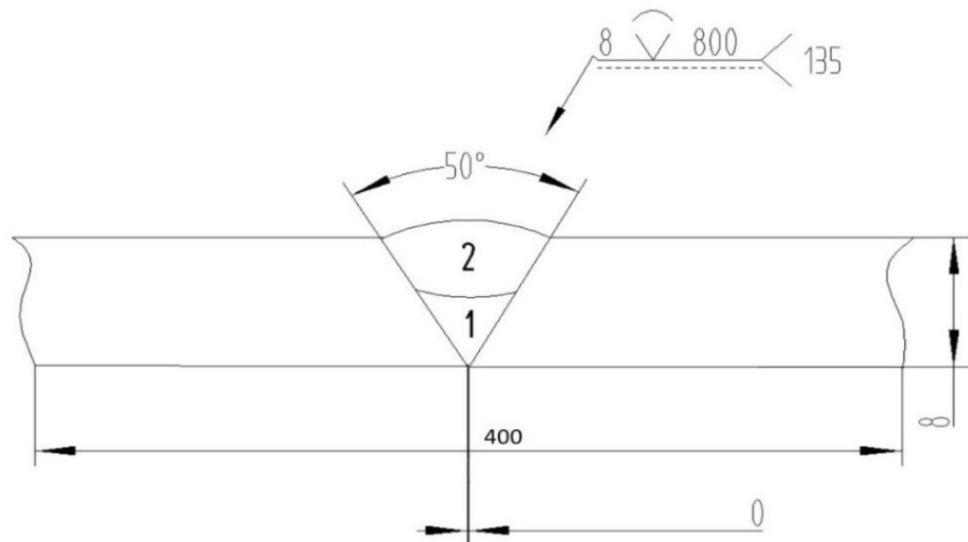


Figure 16 – Joint design.

### 3.2.5 Welding parameters

Wire stand-off distance was 15 mm and Welding torch position of 90° was used for the first run. For the second run, torch position was stinging 80°. Between first and second run cooling time was 40 minutes. Welding procedure specification (WPS) for this weld according to SFS EN-ISO 15609-1:2004 is added in appendix 1. [39] The welding parameters used are presented in table 3.

*Table 3. Welding parameters.*

Run	Wire stand-off distance (mm)	Diameter of filler metal (mm)	Current (A)	Voltage (U)	Wire feed (mm/min)	Travel speed (mm/min)	Heat input (kJ/mm)
1	15	1.0	240	25,7	11,4	9	0,33
2	15	1.0	269	25,8	12,8	6,5	0,51

### 3.3 Testing methods

#### 3.3.1 Optical microscopy

Microstructural analysis of the sample was carried out via optical microscopy. One sample from the weld was gritted with silicon carbide paper from 80 grit to 2500 grit. After gritting sample was polished using 3 and 1  $\mu\text{m}$  size diamond paste, then sample was etched with 2 % percent Nital and ethanol to achieve final and required surface of HAZ and the fusion line. Nital consist 2% nitric acid ( $\text{HNO}_3$ ) and 98% ethanol ( $\text{C}_2\text{H}_5\text{OH}$ ). Optical microscopy was performed using Nikon Epiphot 200 with Nikon Digital Sight DS-U1. Nikon Epiphot 200 is presented in figure 17.



*Figure 17. Nikon Epiphot 200*



### 3.3.2 Scanning electron microscopy

The microstructural features were studied by using Zeiss Ultra 55 scanning electron microscopy (SEM). SEM equipment's used in this study are presented in figure 18.



Figure 18 a) Aalto University's Zeiss Ultra 55 SEM sample unit and in figure 18 b) SEM controls and monitors.

### 3.3.3 Microhardness

Vickers microhardness (HV1) measurement was performed using Buehler NMT-7 digital hardness tester and Omnimet controller unit. Both machines are presented in figure 19. Technique used is categorized as a low-force Vickers hardness test. Mounted sample surface shall be polished and leveled for the proper test. HV1 uses gf1000 test force, which is equal to 9,807 N force. Analyze region for the HV1 indentation mark is 10 to 200  $\mu\text{m}$ . [40]



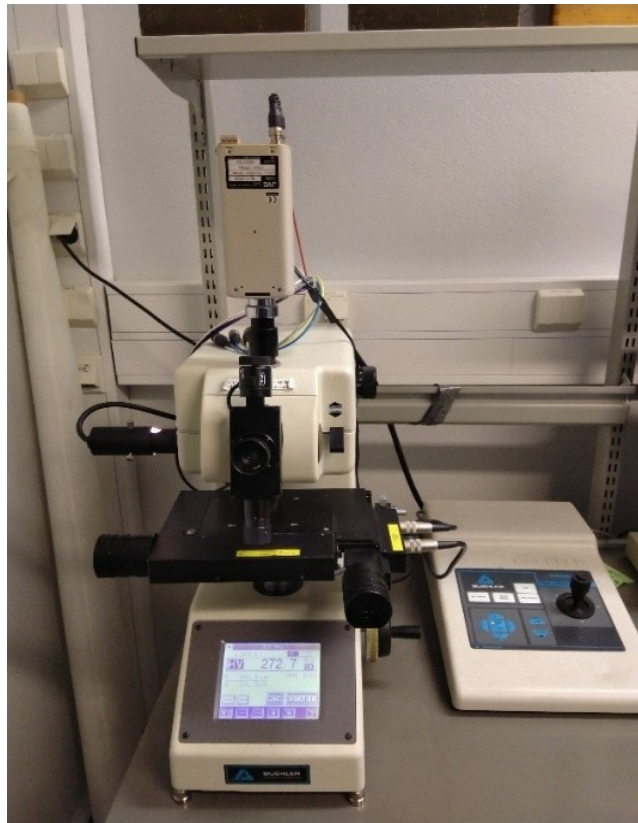


Figure 19. Buehler NMT-7 digital tester and Omnimet control unit.

### 3.3.4 Tensile test

The tensile test is widely used for measuring material properties. Extensometer is placed in the middle section and the extensometer measure elongation during tension. Schematic representation of the tensile test apparatus is presented in figure 20.

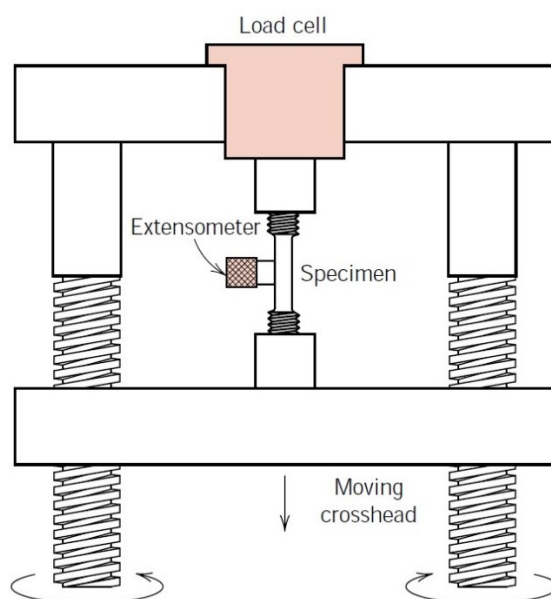


Figure 20. Tensile test apparatus. [27]

Engineering stress is defined by the relationship, where  $A_0$  is the original cross-sectional area and  $F$  is applied force and causes deformation in material. Formula for engineer stress ( $\sigma_{eng}$ ) is presented in equation 7. [41, 42]

$$\sigma_{eng} = \frac{F}{A_0} \quad (7)$$

Transverse tensile test sample according to SFS EN-ISO 4136:2012 is presented in figure 21. Surface roughness value ( $R_a$ ) shall have better than  $5 \mu\text{m}$ , except for the sample ends. [43]

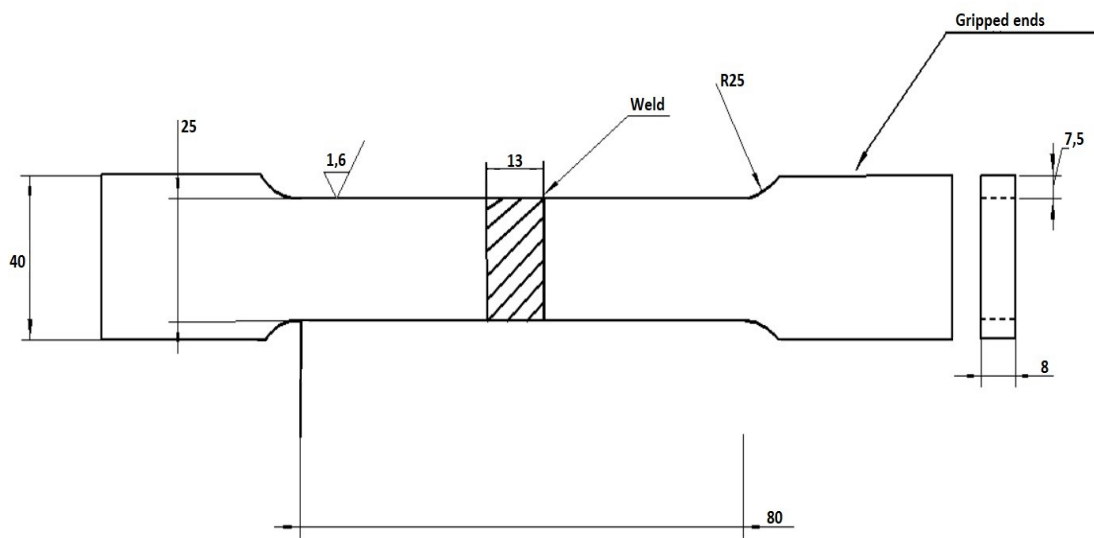


Figure 21 – Rectangular tensile test specimen. [43]

### 3.3.5 Charpy's impact test (CVN)

The Charpy V-notch (CVN) impact toughness test is one of the most commonly used destructive tests (DT). CVN pendulum impact test is a method for determining the energy absorbed (J) in an impact test of metallic materials. [42] The pendulum hammer is released from the off-position and pendulum strikes on the notched specimen of specified temperature. Specimen is placed from both ends to the anvil. The specimen absorbs part of the pendulum's energy. Overall schematic drawing Charpy V-notch impact test set up is presented in figure 22. [27, 44]

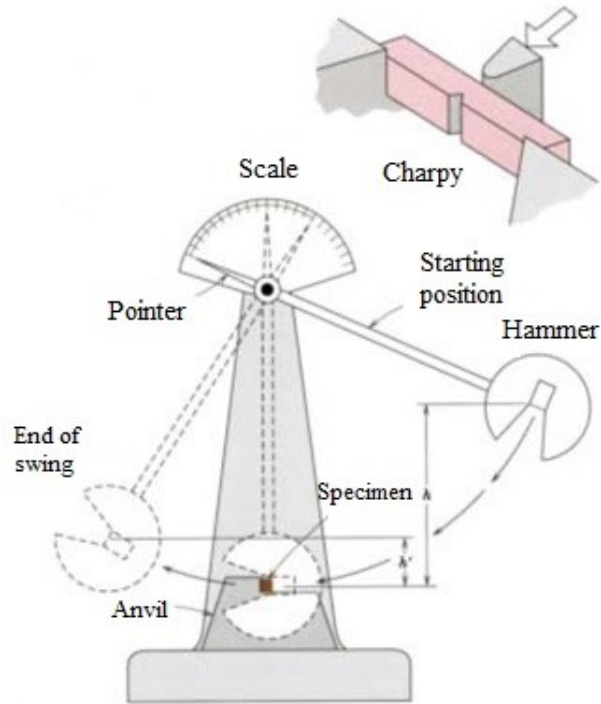


Figure 22. A schematic drawing of a CVN impact testing apparatus. [27]

Full size  $10 \times 10 \times 55$  mm CVN impact toughness test sample dimensions are presented in table 4.

Table 4. Geometrical characteristics of  $10 \times 10 \times 55$  mm sample according to SFS-EN ISO 148-3:2016. [45]

<b>Designation</b>	<b>Value</b>	<b>Tolerance</b>
Length of test piece	55,00 mm	+0,00 – 0,30 mm
Half-length of test piece	27,5 mm	$\pm 0,2$ mm
Width of test piece	10,00 mm	$\pm 0,06$ mm
Thickness of test piece	10,00 mm	$\pm 0,07$ mm
Ligament length	8,00 mm	$\pm 0,06$ mm
Angle of notch	$45,0^\circ$	$\pm 1,0^\circ$

According to SFS EN-ISO 148-1:2016 “If the standard test piece cannot be obtained from the material, one of the sub-size test pieces, having a thickness of 7,5 mm, 5 mm or 2,5 mm, shall be used, if not otherwise specified”. [45] For a  $5 \times 10 \times 55$  and  $7,5 \times 10 \times 55$  mm specimen, required impact values are then reduced to respectively  $2/3$  and  $5/6$  of to make impact energy correspond to a standard-size  $10 \times 10 \times 55$  mm specimen. [46, 47] Dimensions for the sub-sized specimen in this study ( $10 \times 5 \times 55$  mm) is presented in figure 23.

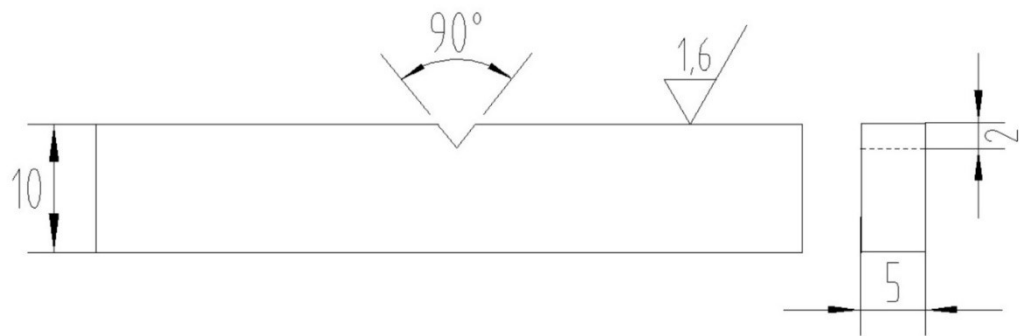


Figure 23. Dimensions of the  $5 \times 10 \times 55$  mm sub-sized specimen used in this study.

In figure 24 is presented impact energy relations with sub-sized ( $5 \times 10$ ) and full-sized ( $10 \times 10$ ) CVN specimens.

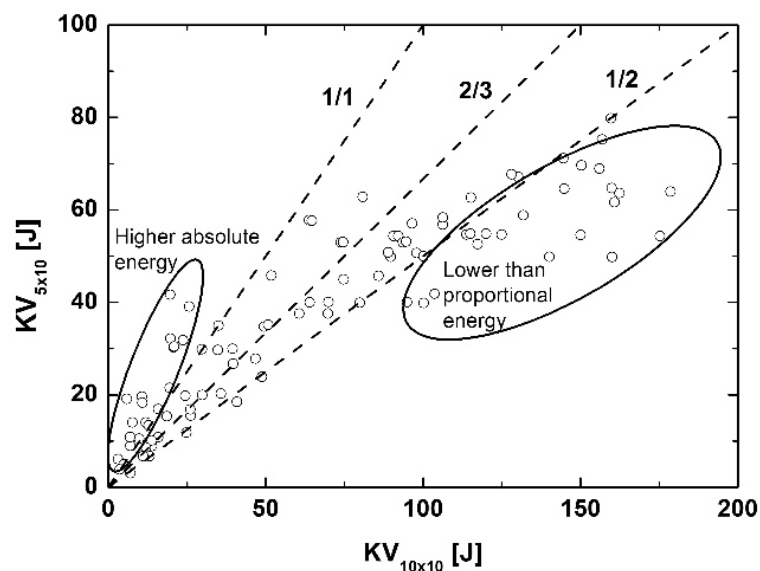


Figure 24. Sub-sized and full-sized CVN specimen energy relations. [46]

### 3.4 Extraction plan for samples

Locations for all test specimens according to SFS EN-ISO 15614-1:2017 are presented in figure 25. Picture of samples is added in appendix 2.

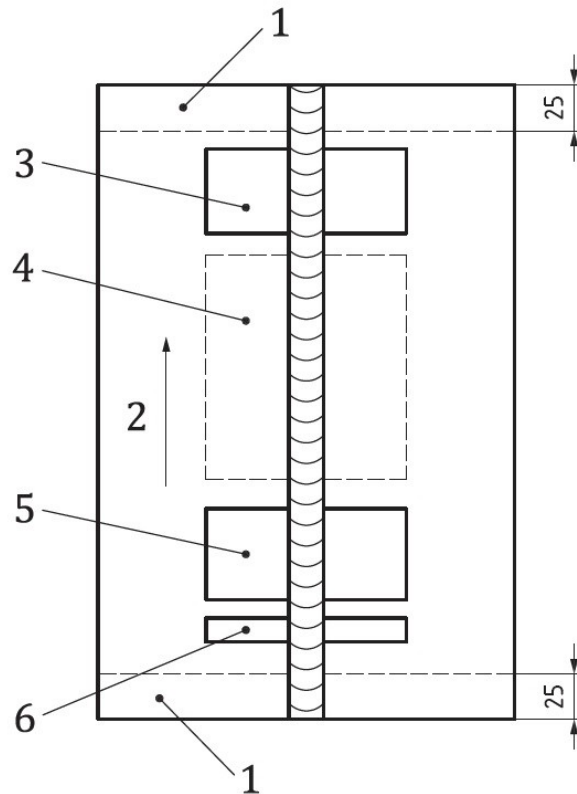


Figure 25 – Sample locations. [48]

- 1 Discard 25 mm (from start and end)
- 2 Welding direction
- 3 Area for: — 1 tensile test specimen and bend test specimens
- 4 Area for: — impact (CVN) and additional test specimens if required
- 5 Area for: — 1 tensile test specimen and bend test specimens
- 6 Area for: — 1 macro test specimen and 1 hardness test specimen.

## 4 Base material results

### 4.1 Optical microscopy

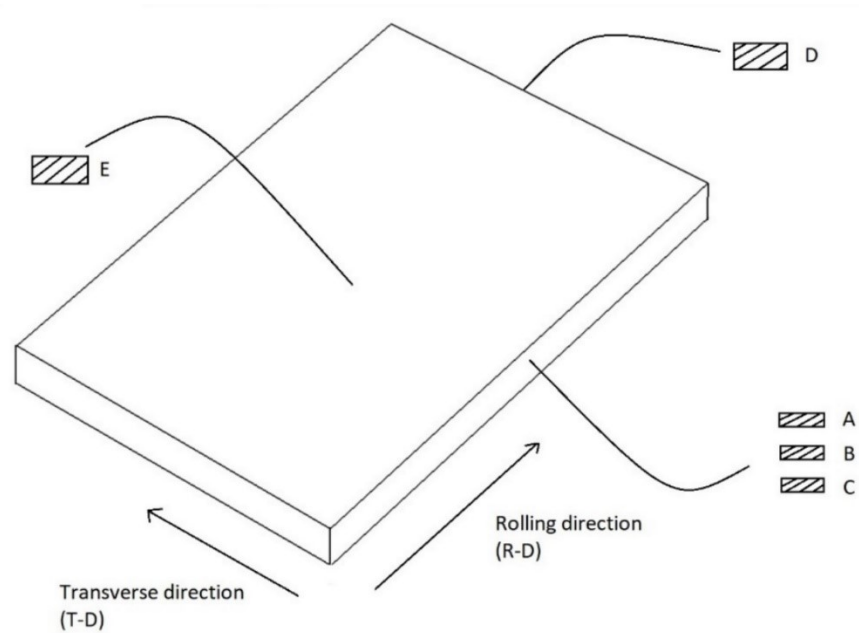


Figure 26. Locations of reference samples extracted from the base material S700MC.

Total of five locations were pictured with microscopy using enlargement, these locations are marked A, B, C, D and E. Location D is presented in figure 26 and picture is 50x enlargement of microstructure.



Figure 27. 50x enlargement of bainitic microstructure from the location D of base material S700MC.



The rest four locations (100x enlargement) of base material are presented in figure A, B, C and E.

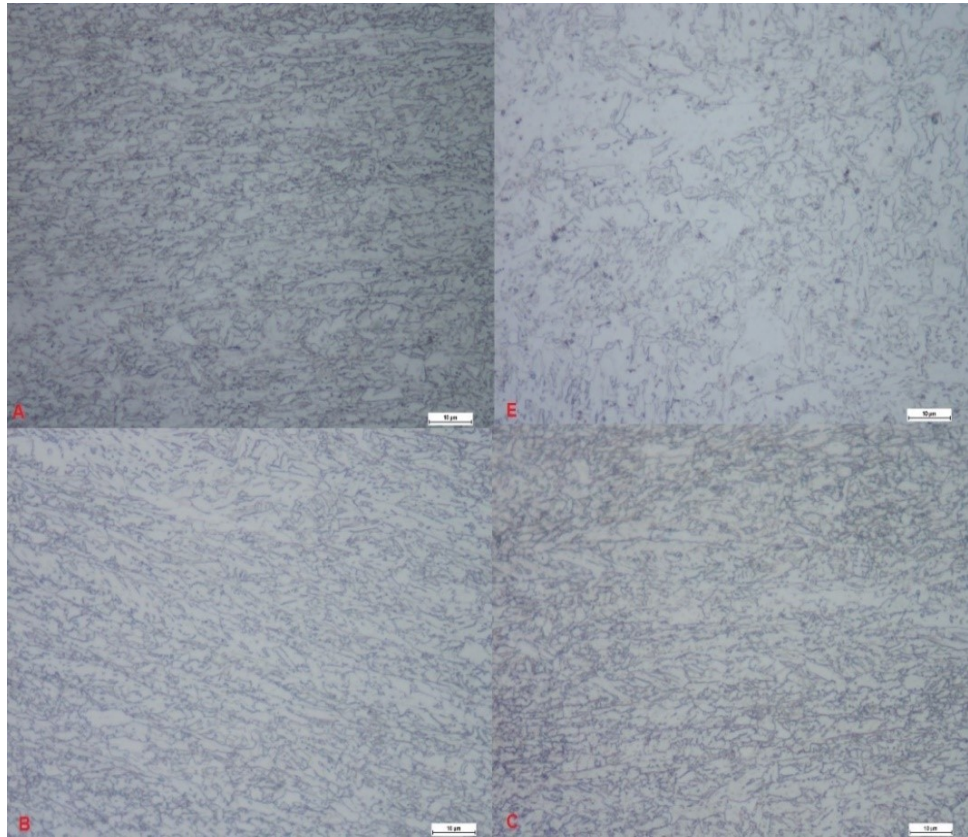


Figure 28. Four (A, B, C, E) 100x enlargement of bainitic microstructure from base material S700MC.

## 4.2 Microhardness

Five Vickers microhardness (HV1) measurement were carried out and average hardness values are presented in table 5.

Table 5. Average microhardness for the base material from locations A, B, C, D and E.

<i>Up1</i>	<i>A</i>	<i>262,3</i>
<i>Middle1</i>	<i>B</i>	<i>257,4</i>
<i>Down1</i>	<i>C</i>	<i>263,8</i>
<i>Plate end / R-D</i>	<i>D</i>	<i>272,1</i>
<i>Middle2</i>	<i>E</i>	<i>277,9</i>

### 4.3 Toughness

Transition curves for sub-sized specimens with the thickness of  $10 \times 5 \times 55$  mm and  $10 \times 7,5 \times 55$  mm were constructed based on the Charpy-V impact test results obtained in the temperature range from  $+20^\circ\text{C}$  to  $-80^\circ\text{C}$ . Results for the base material impact toughness are presented in figures 29 and 30. Formula for standard deviation is presented in equation 7 and standard deviation from data set is added on the curve.

$$S = \sqrt{\frac{(x_1 - \bar{x})^2}{n-1}} \quad (7)$$

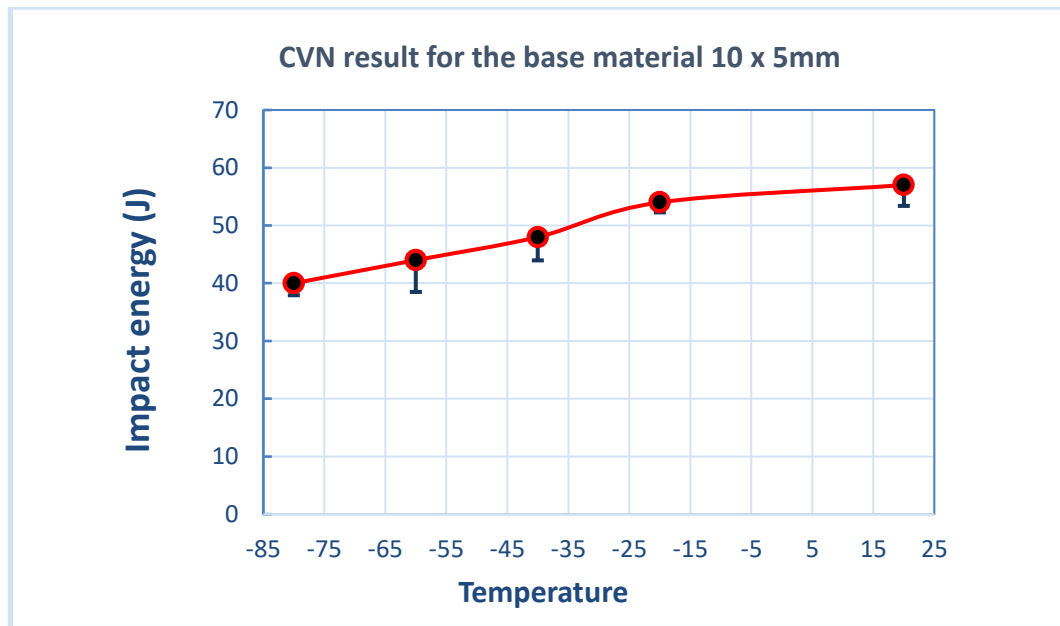


Figure 29. Results for sub-sized  $10 \times 5$  mm CVN samples. Total 15 samples.

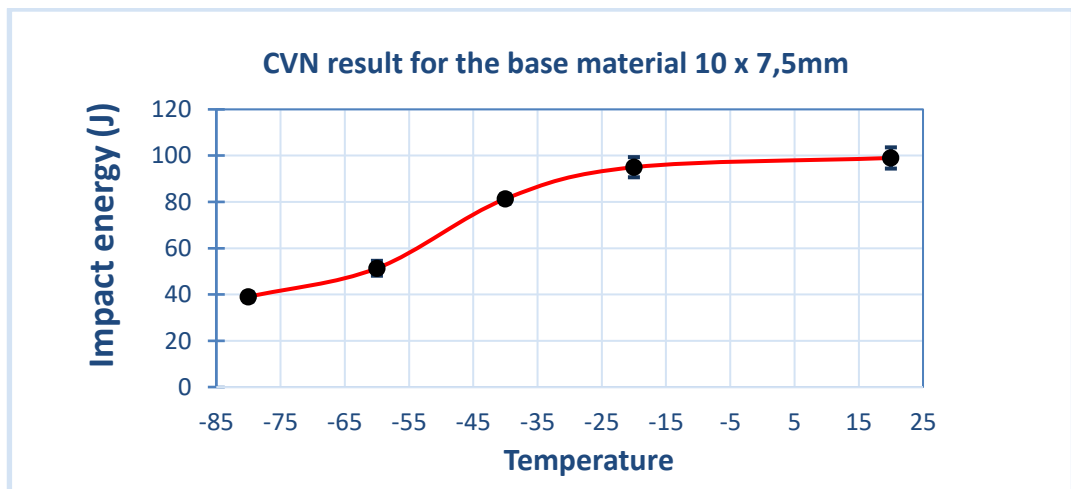


Figure 30. Results for sub-sized  $10 \times 7,5$  mm CVN samples. Total 15 samples.



## 5 Weld joints results

### 5.1 Optical microscopy

Figure 31 shows macrograph and optical microscopic images. White letter boxes indicate location on macrograph.

#### 5.1.1 Macrograph

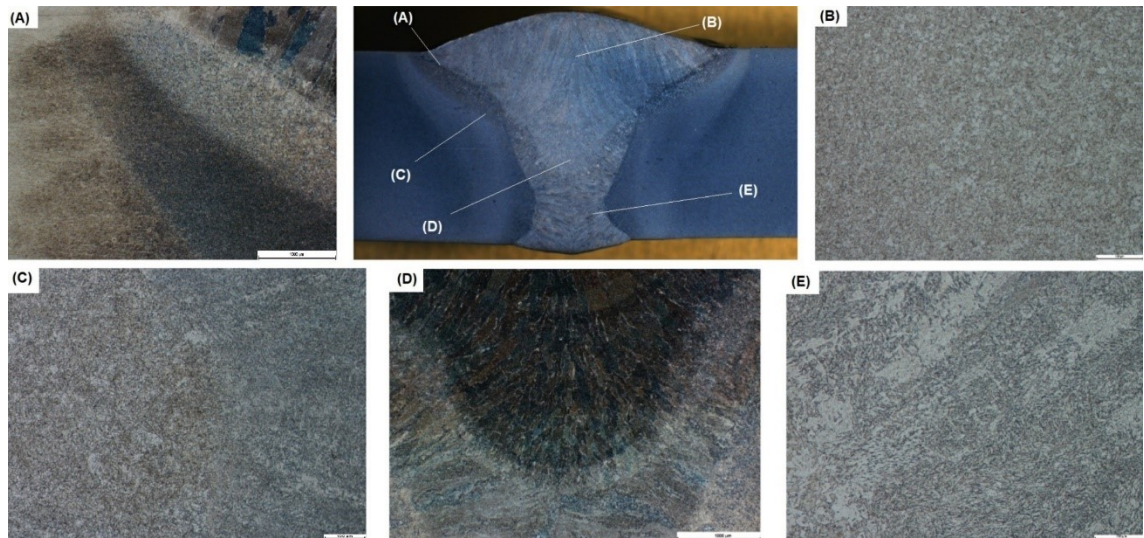


*Figure 31 presents optical macrograph and microscopic images from the different locations of the weld and fusion line. In figures 30 a) and d) blue and brown color is most likely caused by acid (Nital). Figure 30 a) is a 2,5x enlargement of the fusion line and figure 30 b) is 20x enlargement of the weld metal. Figure 30 c) shows the fusion boundary and different grain regions of HAZ with 10x enlargement. Figure 30 d) is shows 2,5x enlargement picture of fusion line and CGHAZ between first weld and second weld. Figure 30 e) shows 20x enlargement overall image of the weld root.*

#### 5.1.2 Micrograph

Optical microscopy pictures were analyzed by location and enlargement. Brittle and ductile “phenomenon” can be seen on microscopy pictures from CVN fracture surfaces. Pictures of interesting samples has added in appendix 4. In figure 32 fusion line boundary in HAZ can be seen.



*Figure 32. Fusion line boundary from left side HAZ. 10x enlargement.*



*Figure 33. Image from the fusion line boundary, right side. 10x enlargement.*

## 5.2 Scanning electron microscopy (SEM)

SEM-pictures were taken from different locations at the right side of HAZ and from two fracture surfaces (samples 35 and 26). Picture 34 shows needle shaped acicular ferrite and many smaller black inclusions can be seen.



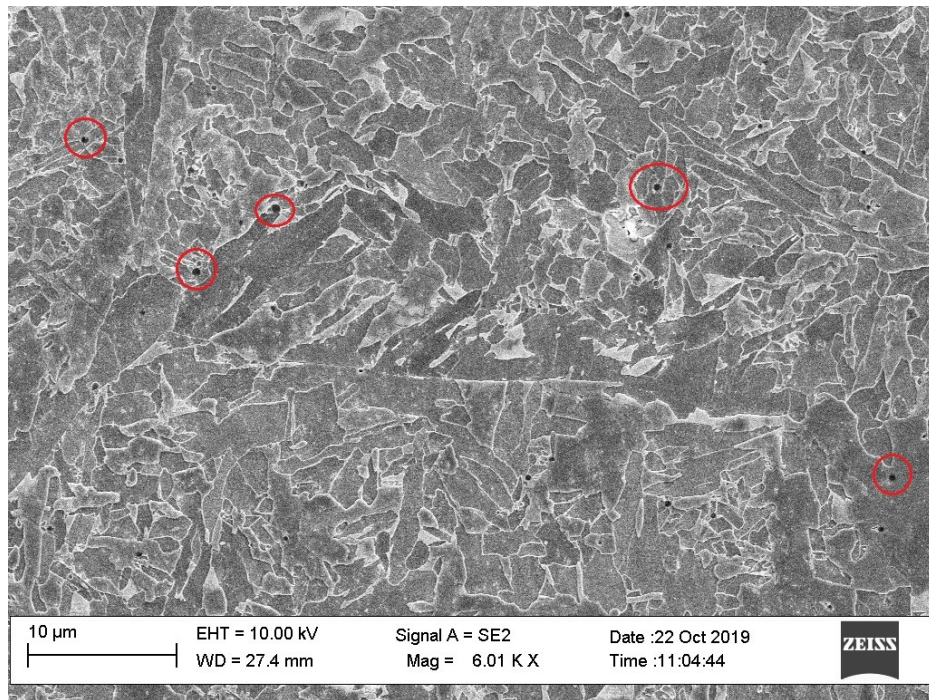


*Figure 34. Acicular ferrite.*

In figure 35 can be seen many microvoids and dimples. This kind of fracture is typical for ductile fracture. This SEM-picture has been taken from sample 35.

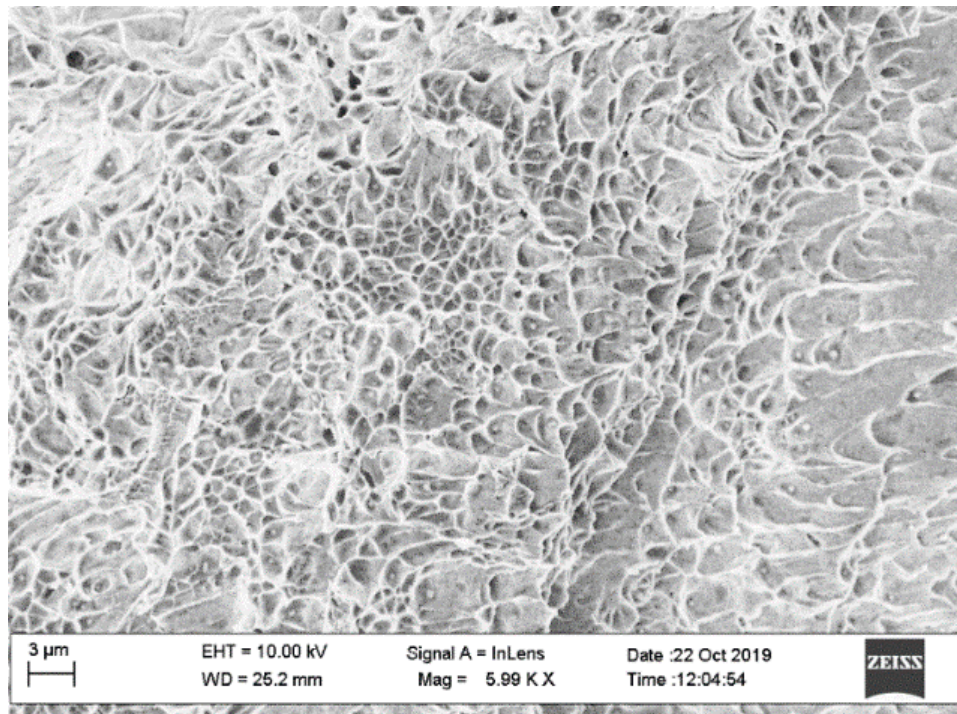


*Figure 35. Microvoids and dimples on fracture surface, sample 35.*

In figure 36 can be seen river like patterns and particles. This kind of fracture is typical for cleavage fracture. This SEM-picture has been taken from sample 26.

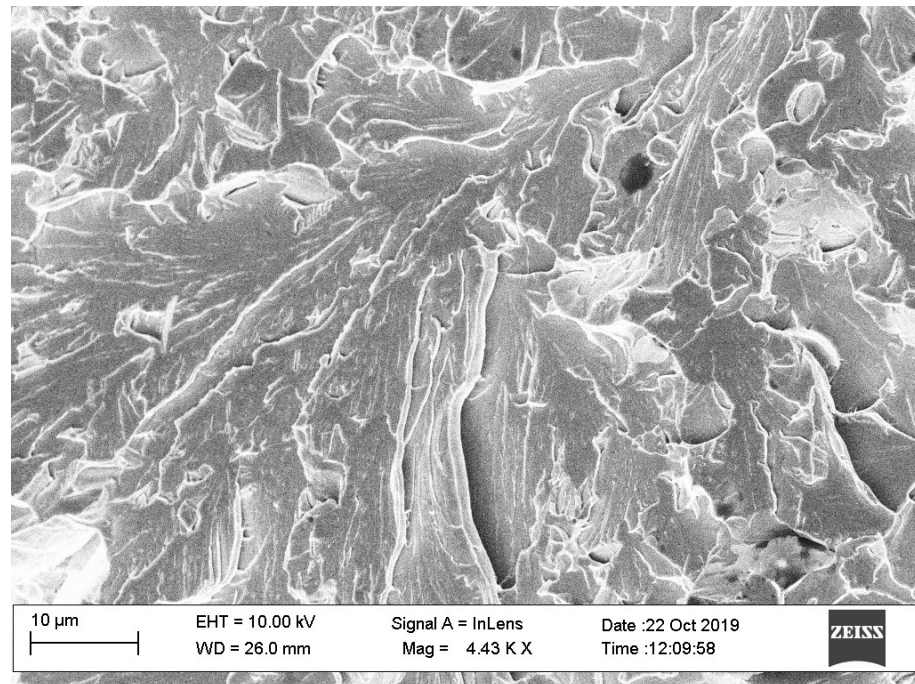


Figure 36. River like patterns on cleavage fracture. Sample 26.

### 5.3 Microhardness

The hardness profile was determined over the welds at 1.5 mm from the face side of the plate and from 1.5 mm of the root side, this is presented in figure 36. The distance between adjacent measuring points was 0.5 mm and the total length of the line consisting of the measuring points was 20 mm.

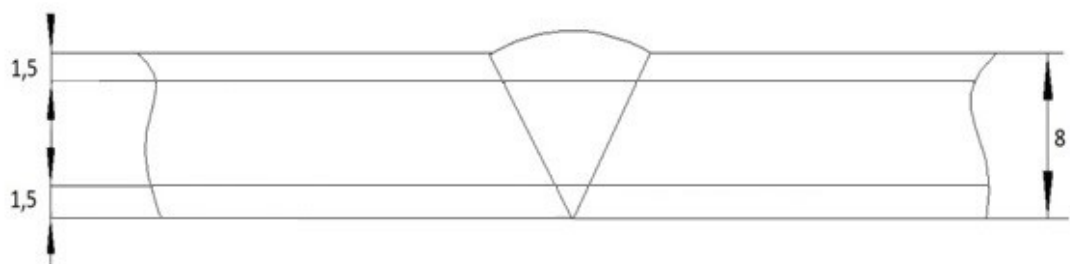


Figure 37. HVI hardness profile of the weld sample.

Hardness measurements were carried out from the weld and the results are presented in figure 38. Zero point in the middle is weld centerline.



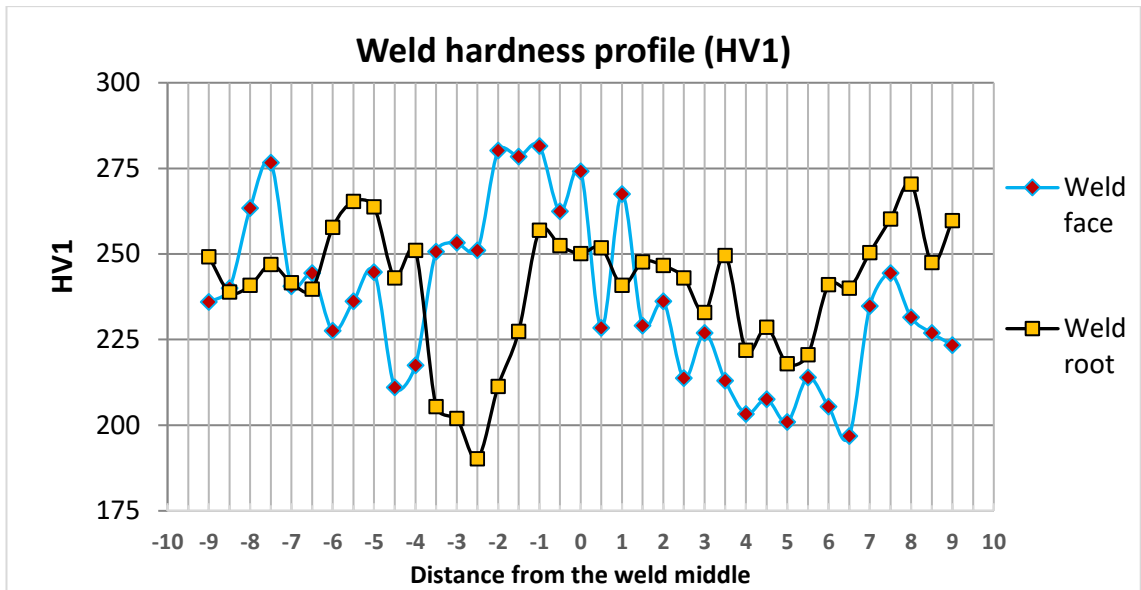


Figure 38. HV1 hardness distribution across the weld.

Figure 39a and graph below shows the softest and the hardest points from the center of weld metal. Face side base line color is blue and root side base line color is yellow. In weld metal, some hardness values are higher than average values from the base material. There is a possibility that face side of the weld contained more alloying elements and this raised weld metal hardenability. Most likely, these elements were supplied along with the filler metal.

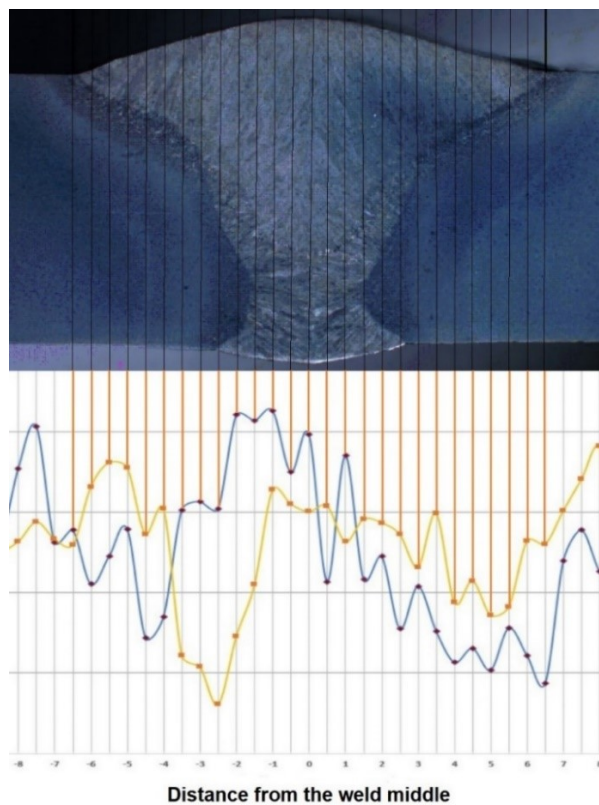


Figure 39. HV1 results and lines on weld from weld center.

## 5.4 Tensile strength

The tensile test was carried out with max load 160 kN when surface area ( $A$ ) was 25 x 8 mm. Tensile test was carried out by Landmark MTS machine, which is presented in figure 40. A 25 mm extensometer was placed to the middle section of the specimen to measure displacement during tension. The original gauge length ( $L_0$ ) was 80 mm.

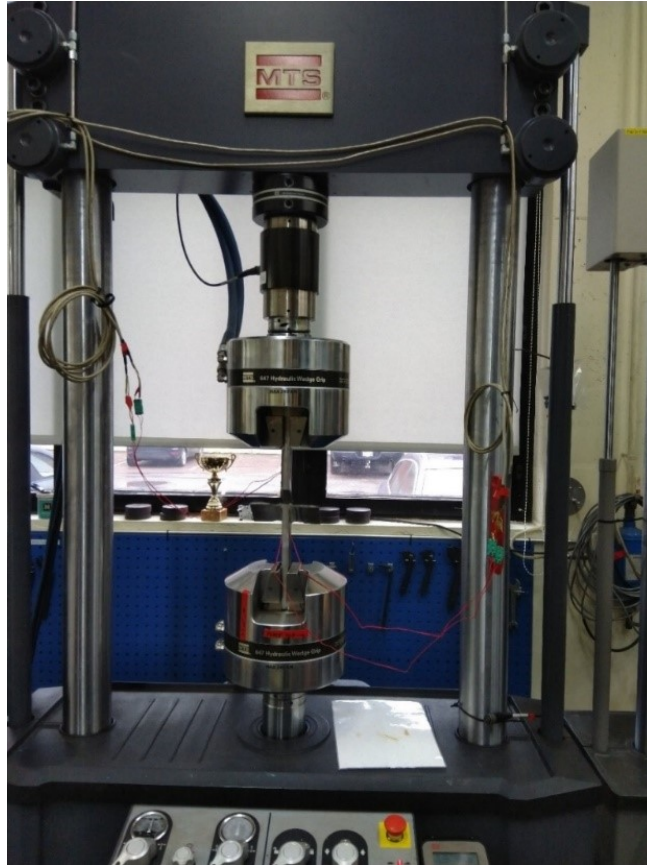


Figure 40. MTS Landmark tensile test machine at Aalto University.

The results for the yield strength ( $R_{p0,2}$ ), tensile strength ( $R_m$ ) and elongation ( $A_0$ ) are presented in table 6. Graph from tensile test is added in appendix 8.

Table 6 – Tensile test results

Yield Strength, ( $R_{p0,2}$ )	Tensile Strength, ( $R_m$ )	Elongation, ( $A_0\%$ )
668	802	10

## 5.5 Charpy's impact test (CVN)

Full-size test sample could not be used in this study because of test material thickness was 8 mm. Sub-sized specimens 5 × 10 × 55 mm from the weld material were used. Notches on the Charpy's sample is presented in figure 41. The notches were placed to center of the weld metal, fusion line minimum, fusion line middle, fusion line max and fusion line max +1, +3- and +5 mm.

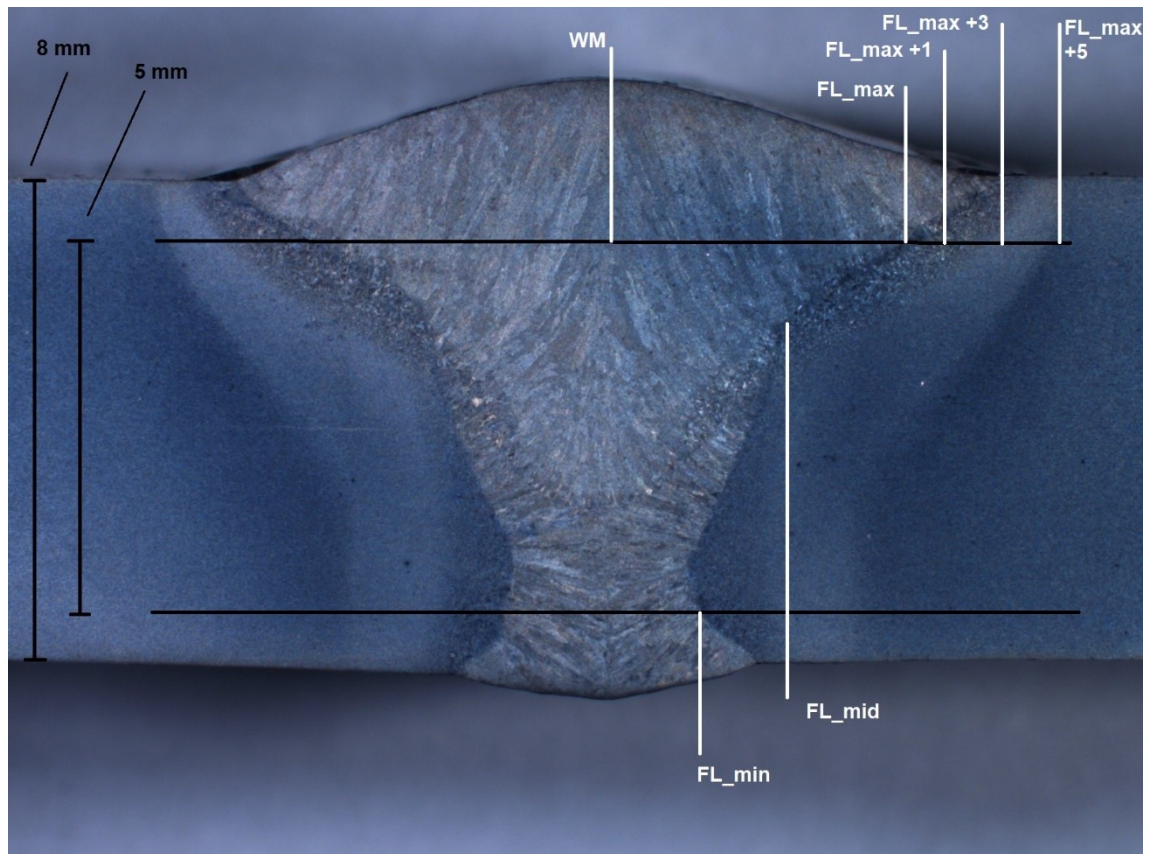


Figure 41.  $10 \times 5 \times 55$  mm sub-sized CVN-impact toughness samples on the weld

In this study, total 51 CVN impact toughness samples from weld material were tested. The CVN data of sub-sized  $10 \times 5$  results from weld are presented in figures 42 – 47. The temperature range was  $-20^{\circ}\text{C}$  to  $-60^{\circ}\text{C}$ .

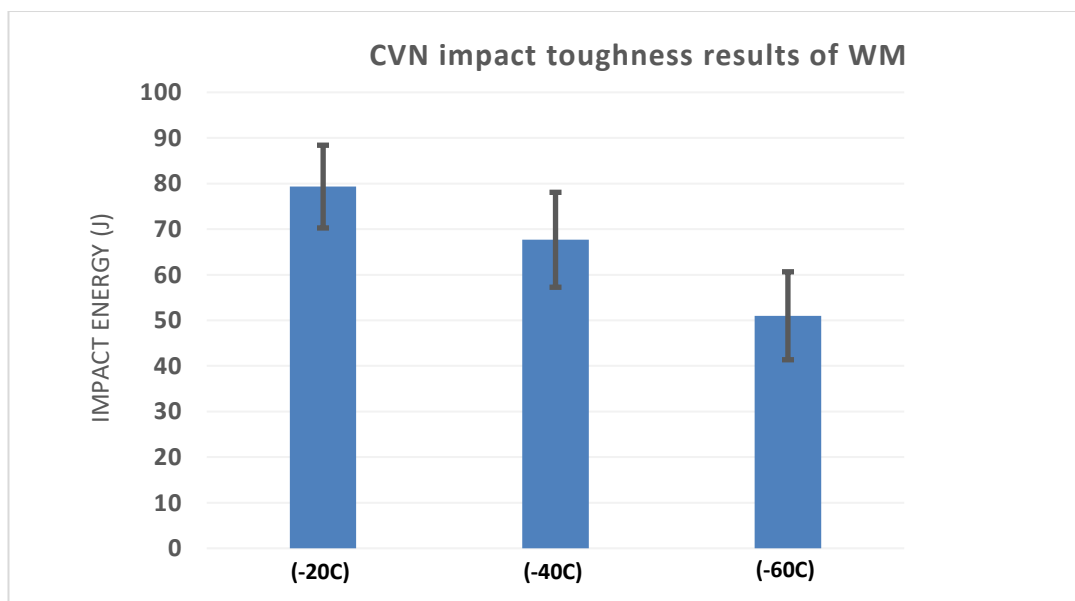


Figure 42. Impact energy of WM.

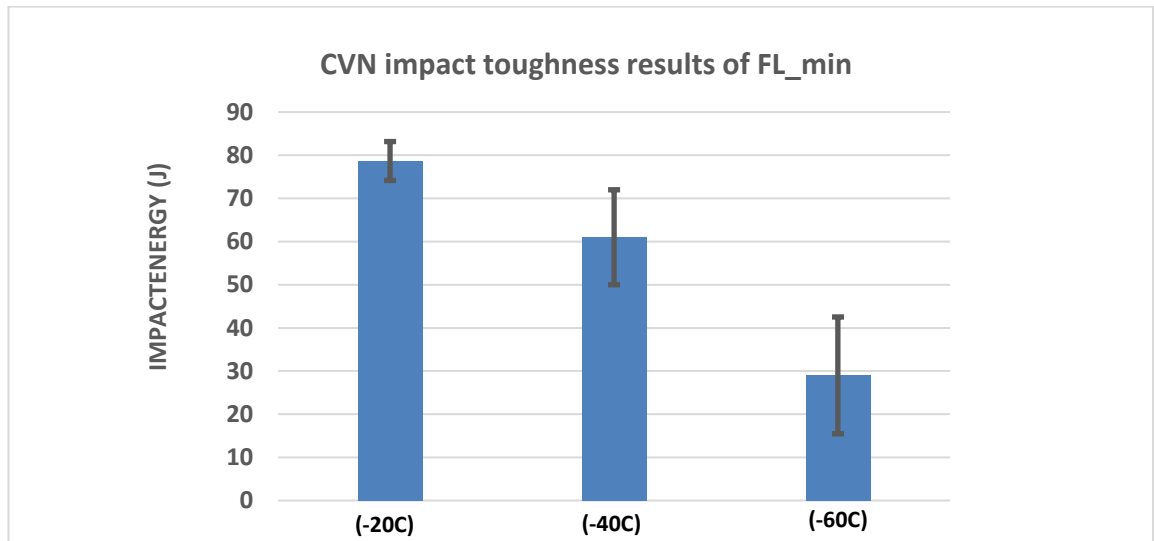


Figure 43. Impact energy of fusion line minimum.

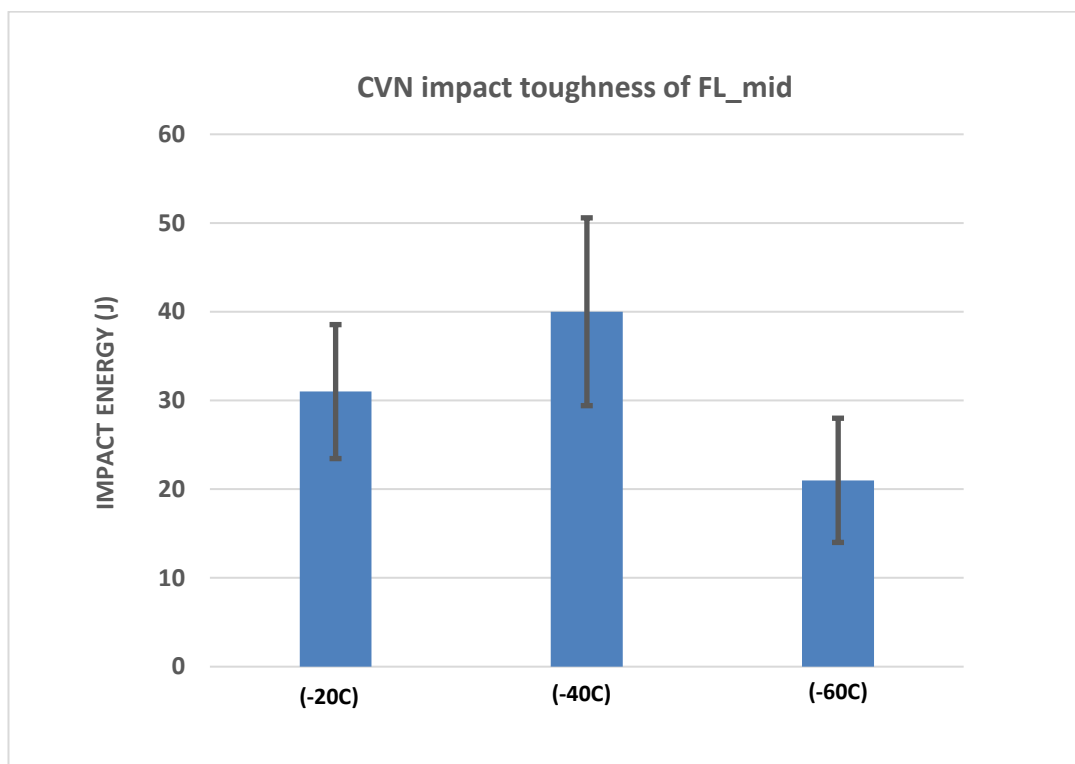


Figure 44. Impact energy of fusion line middle.



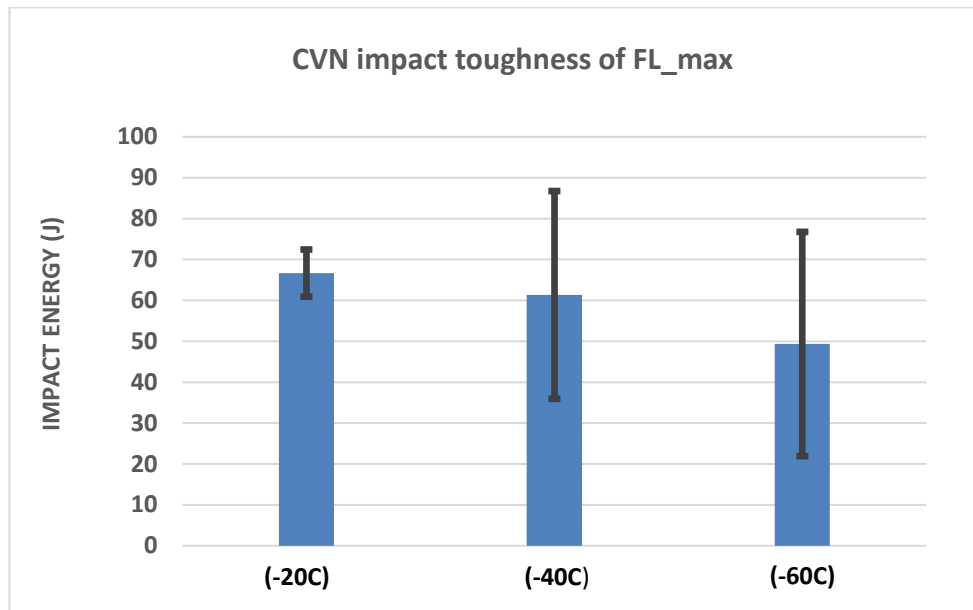


Figure 45. Impact energy of fusion line maximum.

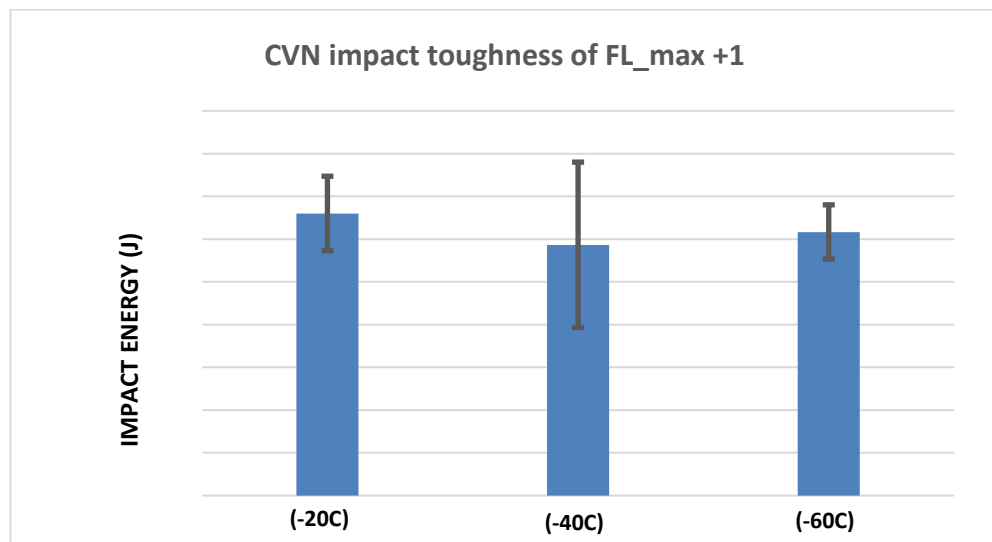


Figure 46. Impact energy of fusion line maximum +1 mm.

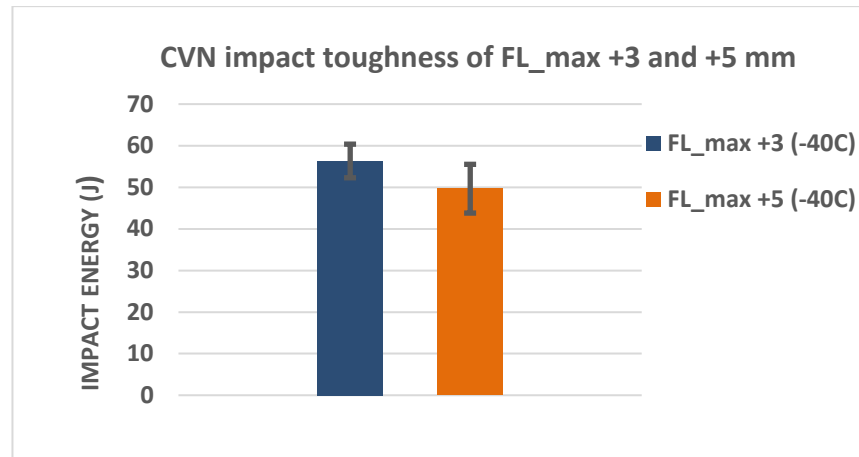


Figure 47. Impact energy of fusion line maximum +3 and +5 mm.

Average impact values in different notch locations are presented in table 7.

	WM	FL_min	FL_mid	FL_max	FL_max +1	FL_max +3	FL_max +5
-20°C	79J	79J	34J	67J	66J	X	X
-40°C	68J	61J	40J	56J	59J	56J	50J
-60°C	51J	29J	21J	49J	62J	X	X

Average microhardness values for sun-sized base material are presented in table 8.

	7,5x10	5x10
20°C	99	57
-20°C	95	54
-40°C	81	48
-60°C	51	44
-80°C	39	40



## 6 Conclusions

As general comment, this master thesis encompassed several tasks in the field of welding technology and materials science. The short period of the research-oriented actions were full of incremental learning steps, and at the end of the process the learning of methods and supporting scientific concepts was the most valuable achievement. In fact, the accuracy of the results, and better processing of the data, would benefit significantly from the opportunity to repeat the procedures based on the learning process.

The main conclusions from the results compiled in this this master thesis are as follows:

- The application of the WPS, does not comprise all the physical and technological conditions that affect the weld result. As an example, in the about 1m length welds the localization and number of the ground clamps does play a significant role in the stability of the electric arc, leading e.g. to lack of penetration or lack of fusion defects. Also the clamping is important in avoiding misalignments of the base materials and the number, position and mass of clamps plays a role in the cooling rates. The weld quality was checked via visual analysis;
- 51 samples were extracted from the welded component with final dimensions of 1000 x 400 x 8 mm produced with the best welding procedure;
- The hardness measured in the base material ranged from 257 HV1 (middle thickness of rolling direction) to 278 HV1 at top surface. In the cross-section to the rolling and welding direction, the value was 272 HV1. Through the thickness the difference was only about 2%, being higher near the surfaces and lower in the middle;
- The toughness in base material show a significant influence from the size of the specimen. In the sub-sized specimen with 7.5 mm there is a clear transition temperature around -50 °C. The scatter is significantly higher in the sub-sized specimen with 5 mm. At -60 °C, the values obtained were for the sub-sized specimen with 7.5 mm = 51 J (61J equivalent in full-size specimen). At -60 °C, the values obtained were for the sub-sized specimen with 5 mm = 44 J (66J equivalent in full-size specimen);
- In the welded specimens the toughness presented a very high scatter, mostly for the -60 °C. This means that problems existed in the precise preparation of the notch location, mostly the ones close to the Fusion Line (min; middle; max).
- The worst values obtained were 16 J to 18 J at -60 °C for the notch located at the fusion line middle and fusion line maximum. According to SFS EN-ISO 10025-6:2009 similar UHSS's impact toughness energy should be higher than 27 J for full size samples, at -40 °C. In this study all average impact toughness values at -40 °C are above 27J;
- From the fractography is noticeable that the lowest toughness results were obtained for straight paths of the crack propagation. This indicates that a tailored design of the WPS and weld joint, avoiding a straight crack propagation will highly improve the joint toughness at the vicinity of the fusion line.

## 7 List of references

- [1] T. Lahtinen, P. Vilaca, P. Peura and S. Mehtonen. 2019. MAG Welding of Modern High Strength Steels with minimum Yield Strength of 700 MPa. *Applied Science*, 9 (5), 1031. 18 pages.
- [2] S. Afkhami, T. Bjork and J. Larkiola. 2019. Weldability of cold-formed high strength steels. *Journal of Constructional Steels Research* 158, pp 86 –98. 12 pages.
- [3] H. Pirinen. 2019. Fatigue strength of welded joints made of S1100 structural steel, Master's thesis, Lappeenranta University of Technology, Finland. 91 pages.
- [4] S. Kou. 2003. *Welding Metallurgy*. Second edition. John Wiley & Sons. 461 pages. ISBN 0-471-43491-4.
- [5] SFS-EN ISO 4063 – 1: 2009. 2011. Welding and allied processes. Nomenclature of processes and reference numbers. Finland. Suomen standardoimisliitto, SFS. 26 pages.
- [6] TÜV (Technischer Überwachungsverein, Germany). Qualification of Welders and Welding Procedures. Accessed 14.11.2019 <https://www.tuv.com/world/en/welding-technology.html>
- [7] American Welding Society, Standard Welding Terms and Definitions, including terms for Adhesive Bonding, Brazing, Soldering, Thermal Cutting, and Thermal Spraying. 12th edition. AWS. 148 pages. ISBN 978-0-87171-763-4. 2009.
- [8] M. Gáspár and A. Balogh. 2013. GMAW Experiments for Advanced (Q+T) High Strength Steels. *Production Processes and Systems, Vol 6*, pp 9–24.
- [9] N. Shikanai, S. Mitao and S. Endo. 2008. Recent Development in Microstructural Control Technologies through the Thermo-Mechanical Control Process (TMCP) with JFE Steel's High-Performance Plates. JFE Technical Report, No. 11. 6 pages.
- [10] SFS EN-ISO 10149 – 1. 2013. Hot rolled flat products made of high yield strength steels for cold forming – Part 1: General technical delivery conditions. Finland. Suomen standardoimisliitto, SFS. 32 pages.
- [11] J. C. Lippold. 2015. *Welding metallurgy and weldability*. John Wiley & Sons. 400 pages. ISBN 978-1-118-23070-1.
- [12] SFS-EN ISO 1011 – 2:2001. Welding. Recommendations for welding of metallic materials. Part 2: Arc welding of ferritic steels. Finland. Suomen standardoimisliitto, SFS. 57 pages.
- [13] SFS-EN ISO 10025 – 1:2004. Hot rolled products of structural steels. Part 1: General technical delivery conditions. Finland. Suomen standardoimisliitto, SFS. 35 pages.
- [14] T. Şükrü. 2010. The assessment of carbon equivalent formulas in predicting the properties of steel weld metals. *Material and Design*, 31 (5), pp 2649 – 2653.

- [15] SFS-EN ISO 1011 – 1: 2009. Recommendations for welding of metallic materials. Part 1: General guidance for arc welding. Suomen standardoimisliitto, SFS. 14 pages.
- [16] M. Mochizuki, T. Shintomi, Y. Hashimoto and M. Toyoda. 2013. Analytical study on deformation and strength in HAZ-Softened welded joints on Fine-Grained-Steels. *Welding in the World*, Vol 48, issue 9–10, pages 2–12.
- [17] P.P.R. Filho, T.S. Cavalcante, V.H. Costa De Albuquerque and J.M.R. Tavares. 2009. Measurement of welding dilution from images using active contours. Accessed 14.11.2019. <https://www.researchgate.net/publication/258031843>
- [18] H. Bhadeshia and R. Honeycombe. Butterworth-Heinemann. 2006. *Steels: Microstructure and Properties*. Third edition. 360 Pages. ISBN 9780750680844.
- [19] T. Bjork, A. Ahola and N. Tuominen. 2018. On the design of fillet welds made of ultra-high-strength steel. *Welding in the World* 62, pages 985 – 995.
- [20] TWI, The Welding Institute Ltd. What is Welding? Accessed 5.10.2019. <https://www.twi-global.com/technical-knowledge/faqs/what-is-welding>
- [21] K. Easterling. 1992. *Introduction to the physical Metallurgy of Welding*. Second edition. Butterworth – Heinemann. 270 pages. ISBN – 13: 978-0750603942.
- [22] O. Vähäkainu and S. Silvennoinen. Otava Oy. 2003. *Rautaruukki Oy, Hitsaajan opas*. 112 pages. ISBN 952-5010-35-X.
- [23] C. J. Davis and E. J. King. 1994. Cleavage initiation in the intercritically reheated coarse-grained heat-affected zone: Part 1. Fractographic evidence. Accessed 13.11.2019. <https://link.springer.com/article/10.1007/BF02651598>
- [24] P. Mohseni, J. K. Sohlberg, M. Karlsen, O. M. Akselsen and E. Ostby. 2012. Investigation of mechanism of cleavage fracture initiation in intercritically coarse-grained heat affected zone of HSLA steel. *Materials Science and Technology* 28 (11), pp 1261-1268.
- [25] Z. Sloderbach and J. Pajak. 2015. Determination of ranges of components of heat affected zone including changes of structure. *Archive of metallurgy and materials*, vol 60, issue 4. 6 pages.
- [26] J. A. Gianetto, J. E. M. Braid, J. T. Bowker and W. R. Tyson. ASME. 1997. Heat-affected zone toughness of a TMCP steel designed for low temperature applications. Accessed 18.11.2019., digital collection, Vol 119, issue 2. 11 pages.
- [27] W. D. Callister, *Fundamentals of Materials Science and Engineering: An Introduction*. 2001. Fifth edition. John Wiley & Sons, Inc. 552 pages. ISBN 0-471-39951-X.
- [28] J. Taavitsainen. 2016. *Weldability of the modern ultra-high strength structural steel*, Master's thesis, Aalto University, Finland. 124 pages.

- [29] T. L. Anderson. 2005. Fracture Mechanics – Fundamentals and Applications, 3rd edition. Third edition. CRC-press. 700 pages. ISBN 0-8493-4260-0. 2005
- [30] E. Schmidova, F. Bozkurt, B. Culek, S. Kumar, L. Kucharikova and M. Uhrick. 2019. Influence of Welding on Dynamic Fracture Toughness of Strenx 700MC Steel. Metals, vol. 9 Issue 5, 494. 15 pages.
- [31] M. Mazur and R. Ulewicz. 2017. Analysis of strength and fatigue properties of construction materials for manufacturing the parts of semi-trailers. Applied Engineering Letters, vol. 2, No 1, pp 32-37, e-ISSN: 2466-4847.
- [32] A. Bhaduri. 2018. Mechanical Properties and Working of Metals and Alloys. Springer series in material science, vol 264, 748 pages.
- [33] SFS-EN ISO 10027 - 1: 2016. Designation systems for steels. Part 1: Steel names. Finland, Suomen standardoimisliitto, SFS. 26 pages.
- [34] Strenx 700MC Plus. SSAB. Data sheet & Chemical Composition (Ladle analysis). Accessed 25.8.2019. <https://www.ssab.com/products/brands/strenx/products/strenx-700-mc-plus>
- [35] Fronius. Cold Metal Transfer welding process, CMT. Accessed 16. 11. 2019. <https://www.fronius.com/en/welding-technology/our-expertise/welding-processes/cmt>
- [36] Böhler Welding by Voestalpine. Welding consumables for Joint Welding. Accessed, 19.10. 2019. <https://www.voestalpine.com/welding/Services/Downloads>
- [37] SFS-EN ISO 14175:2008. Welding consumables. Gases and gas mixtures for fusion welding and allied processes. Finland, Suomen standardoimisliitto, SFS. 9 pages.
- [38] AGA, Linde group. MIG/MAG Welding brochure, PDF, 2014, Finnish. Accessed 1. 11. 2019. [https://www.aga.fi/fi/images/Industrial\\_Gases\\_0818\\_FI\\_tcm634-481224.pdf](https://www.aga.fi/fi/images/Industrial_Gases_0818_FI_tcm634-481224.pdf)
- [39] SFS-EN ISO 15609-1:2004. Specification and qualification of welding procedures for metallic materials. Welding procedure specification. Part 1: Arc welding. Finland, Suomen standardoimisliitto, SFS. 7 pages.
- [40] Vickers. SFS EN-ISO 6507 - 1: 2018. Metallic materials – Vickers hardness test for metallic materials. Test method. Finland, Suomen standardoimisliitto, SFS. 30 pages.
- [41] SFS-EN ISO 6892-1:2016. Metallic materials. Tensile testing. Part 1: Method of test at room temperature. Suomen standardoimisliitto, SFS, 83 pages.
- [42] R. W. Hertzberg, J. L. Hertzberg and R. P. Vinci. 2012. Deformation and fracture mechanics of engineering material. Fifth edition. John Wiley & Sons. 784 pages. ISBN: 978-0-470-52780-1.
- [43] SFS EN-ISO 4136:2012. Destructive tests on welds in metallic materials. Transverse tensile test. Finland, Suomen standardoimisliitto, SFS. 21 pages.

[44] SFS-EN ISO 148 - 1: 2016. Metallic materials - Charpy pendulum impact test - Part 1: Test method. Finland, Suomen standardoimisliitto, SFS. 35 pages.

[45] SFS-EN ISO 148 - 3: 2016. Metallic materials - Charpy pendulum impact test - Part 3: Preparing and characterization of Charpy V-notch test pieces for indirect verification of pendulum impact machines. Finland, Suomen standardoimisliitto, SFS. 25 pages.

[46] K. Wallin, P. Karjalainen – Roikonen and P. Suikkanen. 2016. Sub-sized CVN specimen conversion methodology. European conference on fracture (ECF 21). Procedia Structural Integrity 2, pp 3735 – 3742.

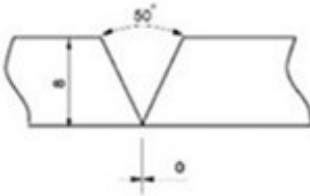
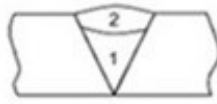
[47] Det Norske Veritas. DNV Off-Shore Standard, OS-B101. 2009. Metallic Materials, 49 pages. Accessed 18.11.2019.<https://rules.dnvgl.com/docs/pdf/DNV/codes/docs/2009-04/Os-B101.pdf>

[48] SFS-EN ISO 15614-1:2017. Specification and qualification of welding procedures for metallic materials. Welding procedure test. Part 1: Arc and gas welding of steels and arc welding of nickel and nickel alloys. Finland, Suomen standardoimisliitto, SFS. 46 pages.



## Appendix 1

## Welding Procedure Specification (WPS). ISO 15609-1:2004

Consumables		Base Material	
Welding process (root): - Consumable: - Specification:	<b>Böhler X70-IG</b> <b>Mison S (M20)</b>	Parent Material: <b>W01, S700MC. (CEN ISO/TR 15608:2017)</b>	
Welding process (fill): - Consumable: - Specification:	<b>Böhler X70-IG</b> <b>Mison S (M20)</b>	Thickness: <b>8 mm</b>	
Joint Details		Joint Position	
Joint Type: <b>Butt weld, ss, nb.</b> Manual/Mechanised: <b>Mechanised</b>		Welding Position: <b>PA (SFS-EN ISO 6947)</b>	
Joint Sketch			
			

## Welding Details

Run	Process	Consumable	Diameter mm	Current A	Voltage V	Type of current / Polarity	Wire Feed Speed m/min	Heat Input kJ/mm
1	135	X70-IG	1,0	241	25,8	DC+	11,4	0,33
2	135	X70-IG	1,0	258	28,9	DC+	12,8	0,51

Details of Back Gouging/Backing: <b>NA</b>
Preheat Temperature: <b>NA</b> Interpass Temperature: <b>Room (23C)</b>
Post-Weld Heat Treatment: <b>NA</b> Temperature: Time:

## Notes:

Welding time for first pass, 88,3 s.  
Welding time for second pass 124,1 s.  
Travel speed (v) for root, 9mm/s.  
Travel speed (v) for fill, 6,5mm/s.  
Wire stand-off distance 15 mm.  
Torch angle for second run 80-degree stinging.  
Gas flow rate 18L/min.  
1st pass average I = 241A, U = 25,8V.  
2nd pass average I = 258A, U = 25,8V.

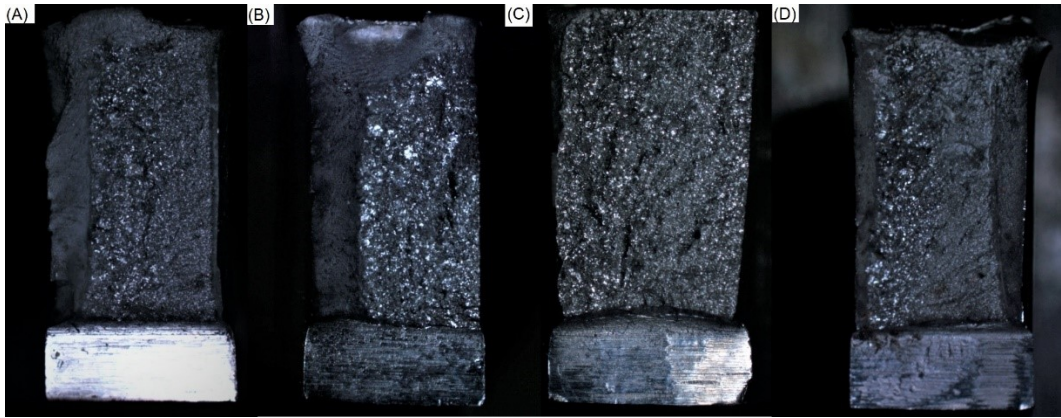


## Appendix 3

Sample	Joules	Location	Temp.
1.	71	WM	-20
2.	76	WM	-40
3.	55	WM	-60
4.	79	FL_MIN	-20
5.	72	FL_MIN	-40
6.	28	FL_MIN	-60
7.	30	FL_MID	-20
8.	48	FL_MID	-40
9.	29	FL_MID	-60
10.	70	FL_MAX	-20
11.	76	FL_MAX	-40
12.	69	FL_MAX	-60
13.	72	FL_MAX +1	-20
14.	55	FL_MAX +1	-40
15.	58	FL_MAX +1	-60
16.	67	FL_MAX +3	-40
17.	43	FL_MAX +5	-40
18.	78	WM	-20
19.	56	WM	-40
20.	40	WM	-60
21.	83	FL_MIN	-20
22.	61	FL_MIN	-40
23.	43	FL_MIN	-60
24.	24	FL_MID	-20
25.	28	FL_MID	-40
26.	16	FL_MID	-60
27.	70	FL_MAX	-20
28.	76	FL_MAX	-40
29.	61	FL_MAX	-60
30.	56	FL_MAX +1	-20
31.	61	FL_MAX +1	-40
32.	58	FL_MAX +1	-60
33.	60	FL_MAX +3	-40
34.	54	FL_MAX +5	-40
35.	89	WM	-20
36.	71	WM	-40
37.	58	WM	-60
38.	74	FL_MIN	-20
39.	50	FL_MIN	-40
40.	16	FL_MIN	-60
41.	39	FL_MID	-20
42.	44	FL_MID	-40
43.	18	FL_MID	-60
44.	60	FL_MAX	-20
45.	32	FL_MAX	-40
46.	18	FL_MAX	-60
47.	70	FL_MAX +1	-20
48.	60	FL_MAX +1	-40
49.	69	FL_MAX +1	-60
50.	52	FL_MAX +3	-40
51.	52	FL_MAX +5	-40

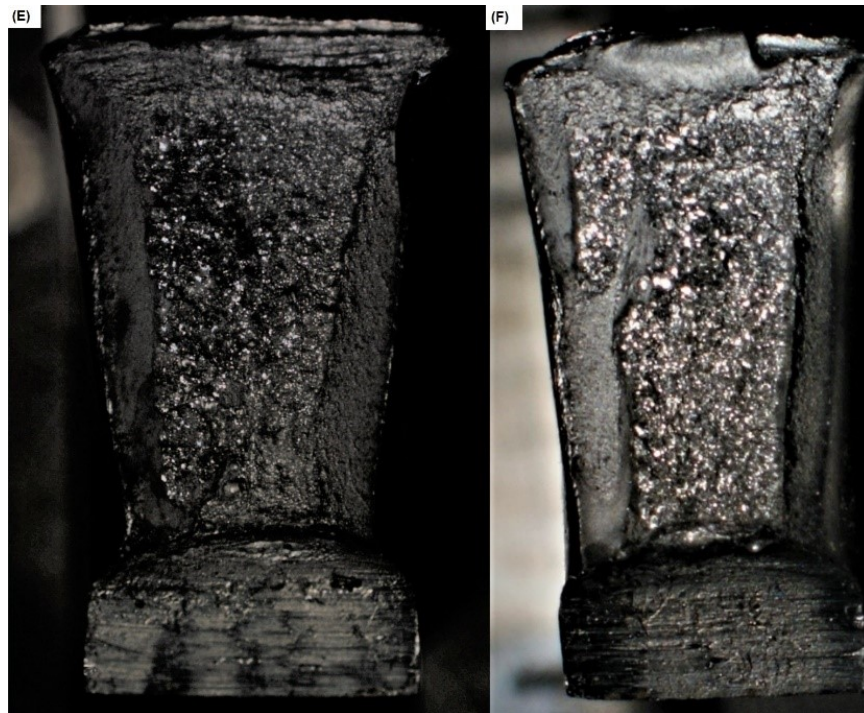


## Appendix 4 a)



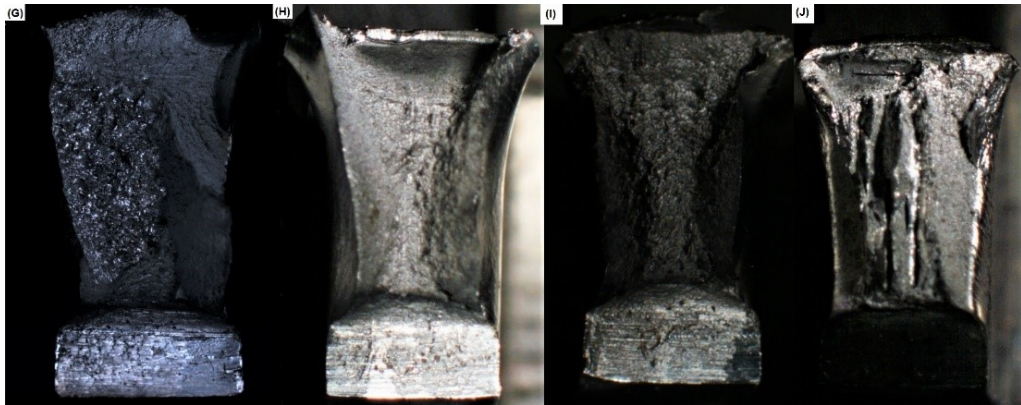
*Brittle samples and lowest impact results at -60°C. A) Sample 43 (18J, FL\_max). B) Sample 40 (16J, FL\_min). C) Sample 26 (16 J, FL-middle) and D) sample 46 (18J, FL-middle).*

## Appendix 4 b)



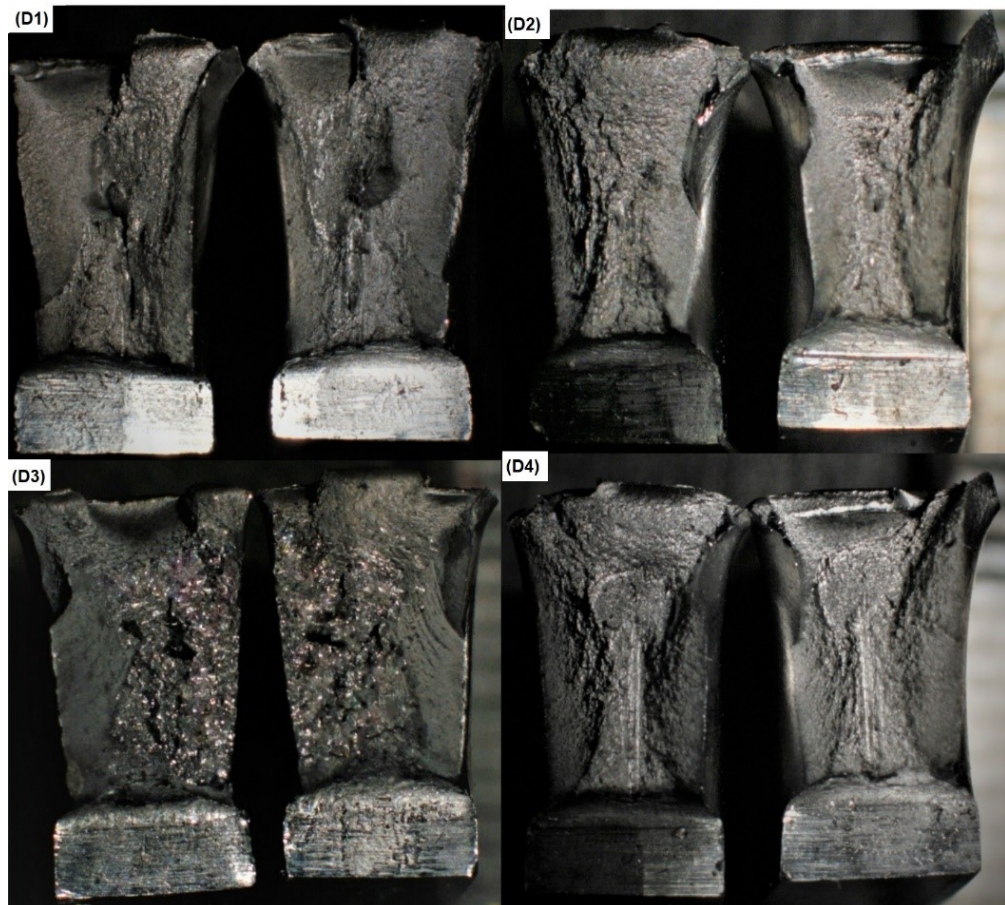
*Brittle samples at -20°C. E) sample 24 (24J, FL\_middle). F) Sample 41 (39J, FL\_middle).*

## Appendix 4 c)



Fracture surfaces at  $-40^{\circ}\text{C}$ . G) Sample 5 (72J,  $FL_{min}$ ). H) Sample 28 (76J,  $FL_{max}$ ). I) Sample 39 (50J,  $FL_{max} + 3\text{mm}$ ) and J) sample 50 (50J,  $FL_{max} + 3\text{mm}$ ).

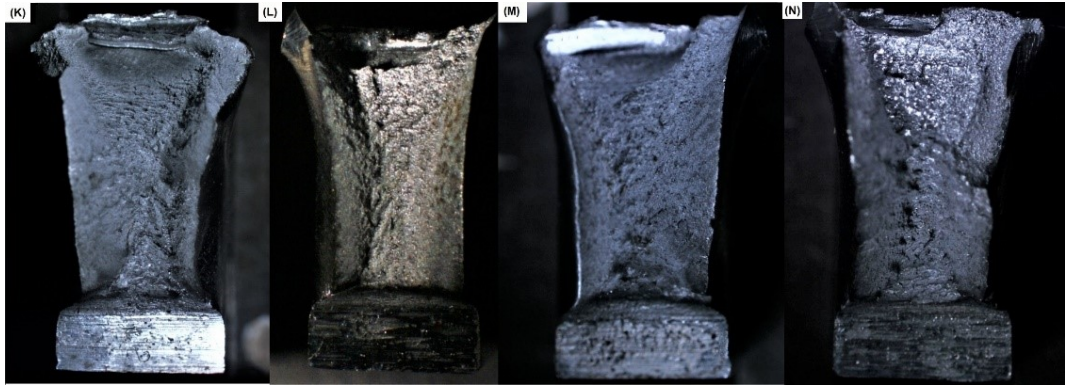
## Appendix 4 d)



Fracture surfaces at  $-60^{\circ}\text{C}$ . D1) Sample 15 (58J,  $FL_{max} + 1\text{mm}$ ). D2) Sample 49 (69J,  $FL_{max} + 1\text{mm}$ ). D3) Sample 20 (40J, WM) and D4) sample 32 58J,  $FL_{max} + 1\text{mm}$ .

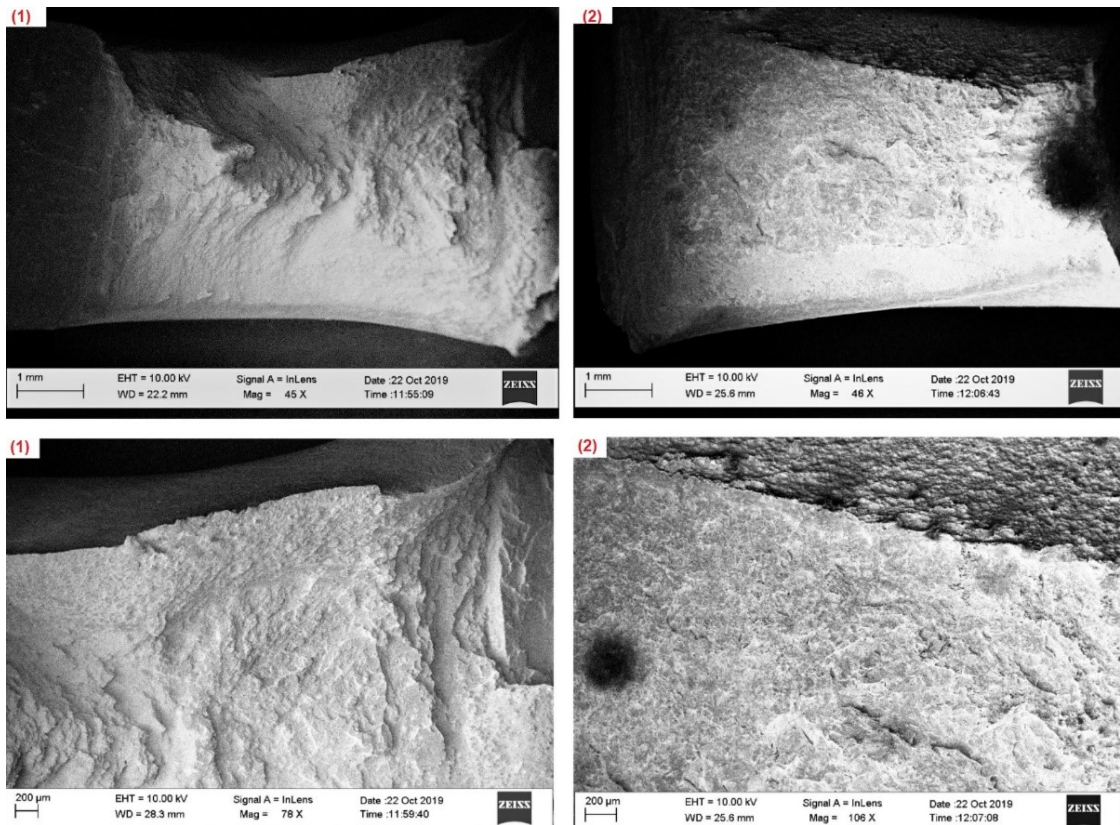


## Appendix 4 e)



*Samples at -20°C. K) Sample 4 (79J, FL\_min). L) Sample 12 (72J, FL\_max +1mm.). M) Sample 21 (83J, FL\_min). N) Sample 35 with highest impact result (89 J, WM).*

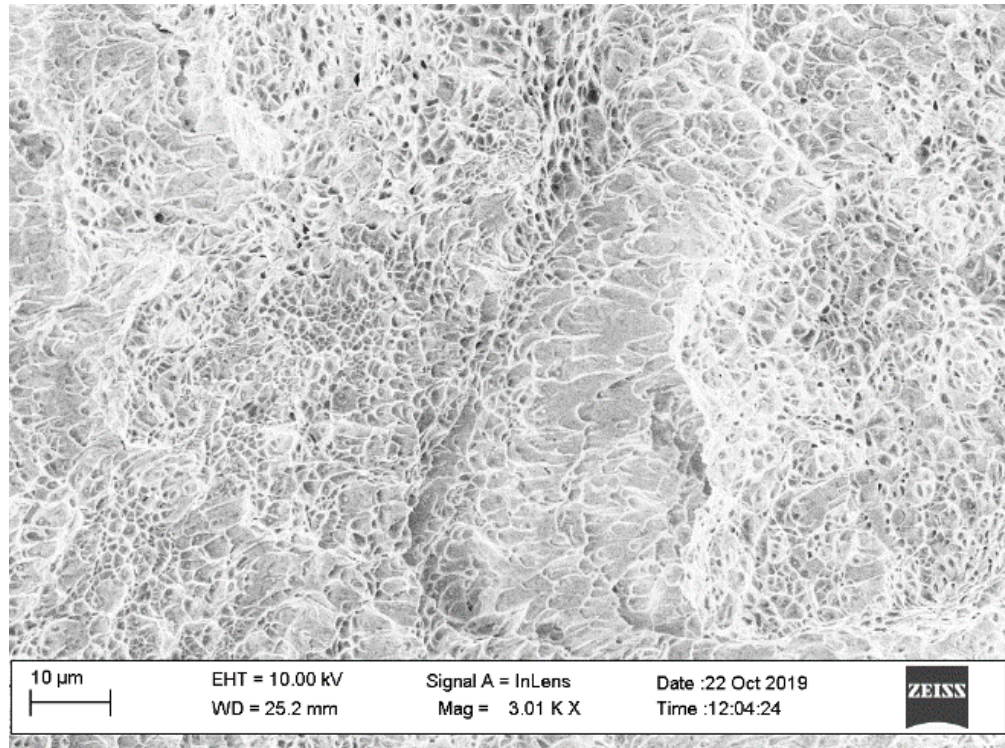
## Appendix 5 a)



*SEM picture from ductile sample 35. Sample 35, highest impact result (89 J, WM, -20°C). SEM picture from brittle sample 26. Sample 26, lowest impact result (16 J, FL-middle, -60°C).*

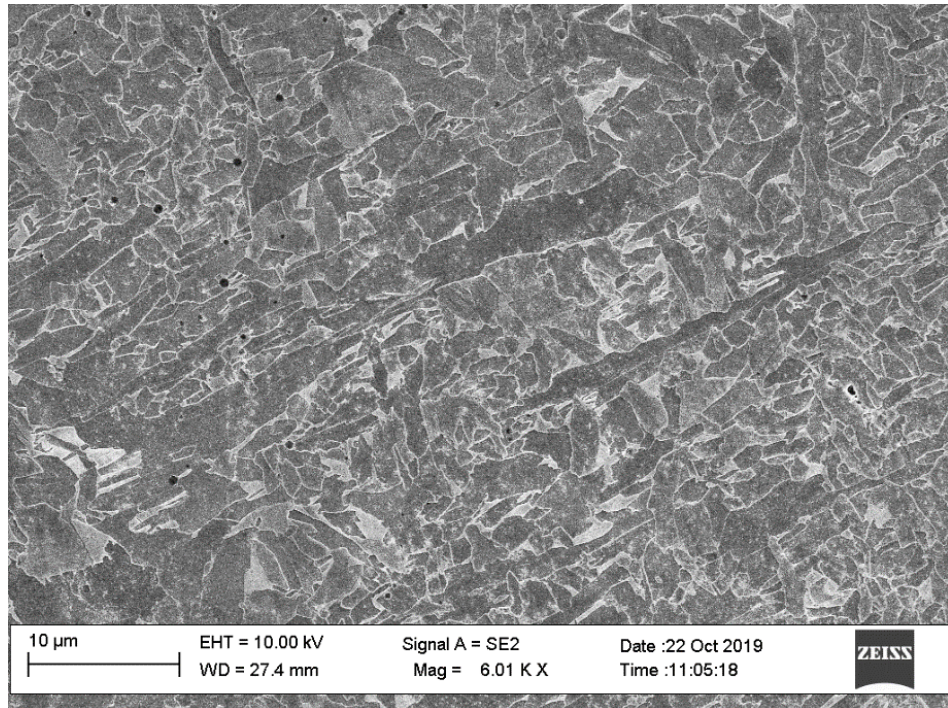


## Appendix 5 b)



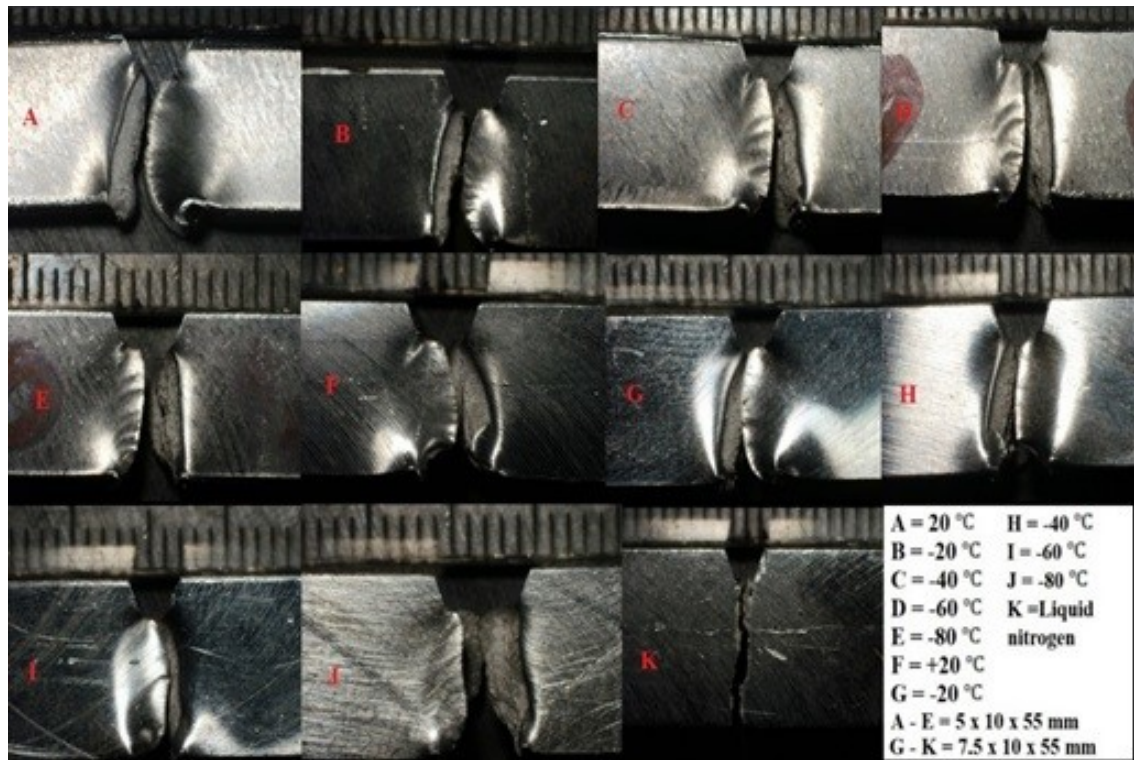
*Ductile sample 35 from S700MC weld.*

## Appendix 5 c)



*Partially austenitization zone of HAZ from S700MC weld.*

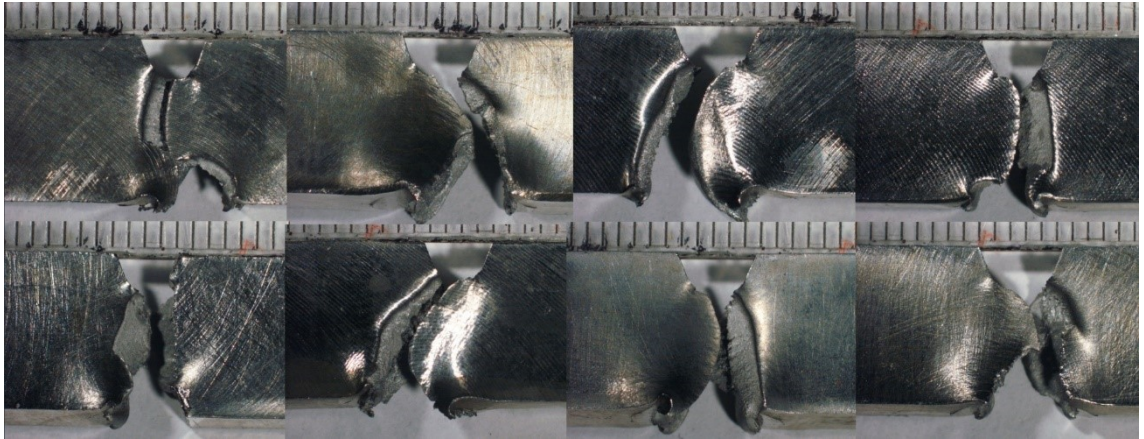
## Appendix 6



*Side profiles of base material 10 × 5 × 55 mm and 10 × 7,5 × 55 mm.*

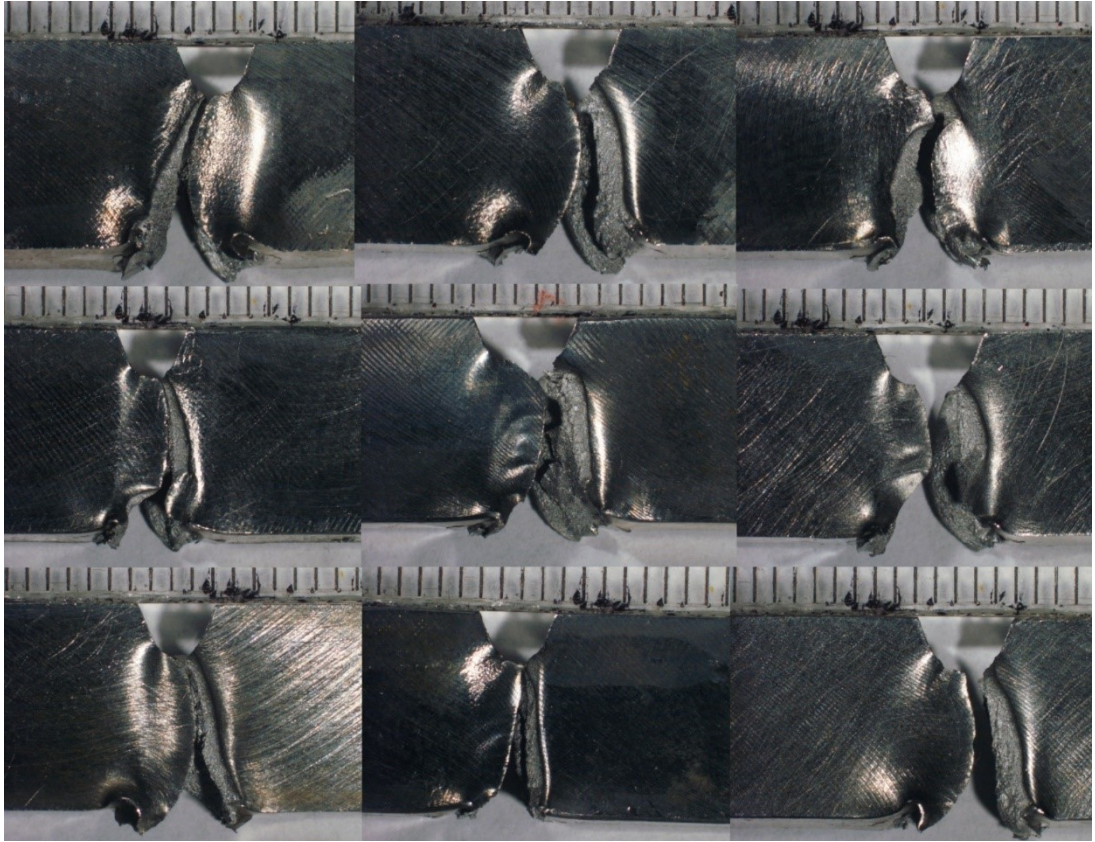


## Appendix 7 a)



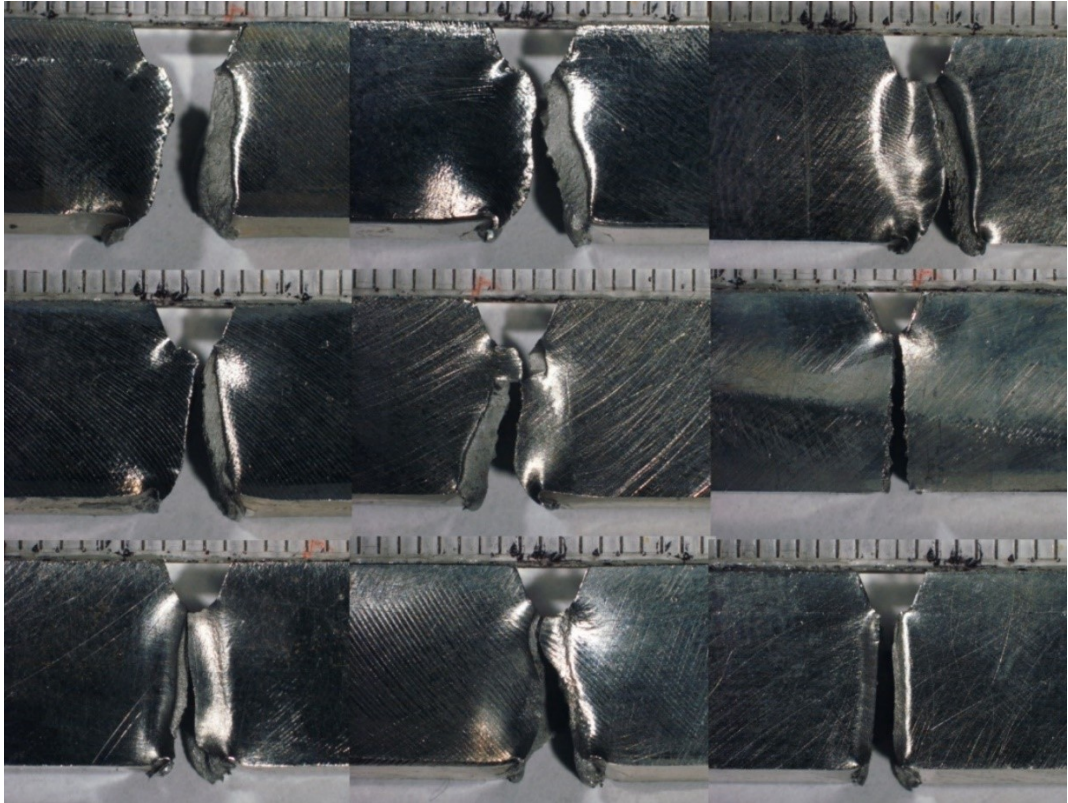
*Weld material. Samples 1, 2, 18, 19, 20, 35, 36 and 37.*

## Appendix 7 b)



*Fusion line\_min. Samples 4, 5, 6, 21, 22, 23, 38, 39 and 40.*

## Appendix 7 c)



*Fusion line\_middle. Samples 7, 8, 9, 24, 25, 26, 41, 42 and 43.*



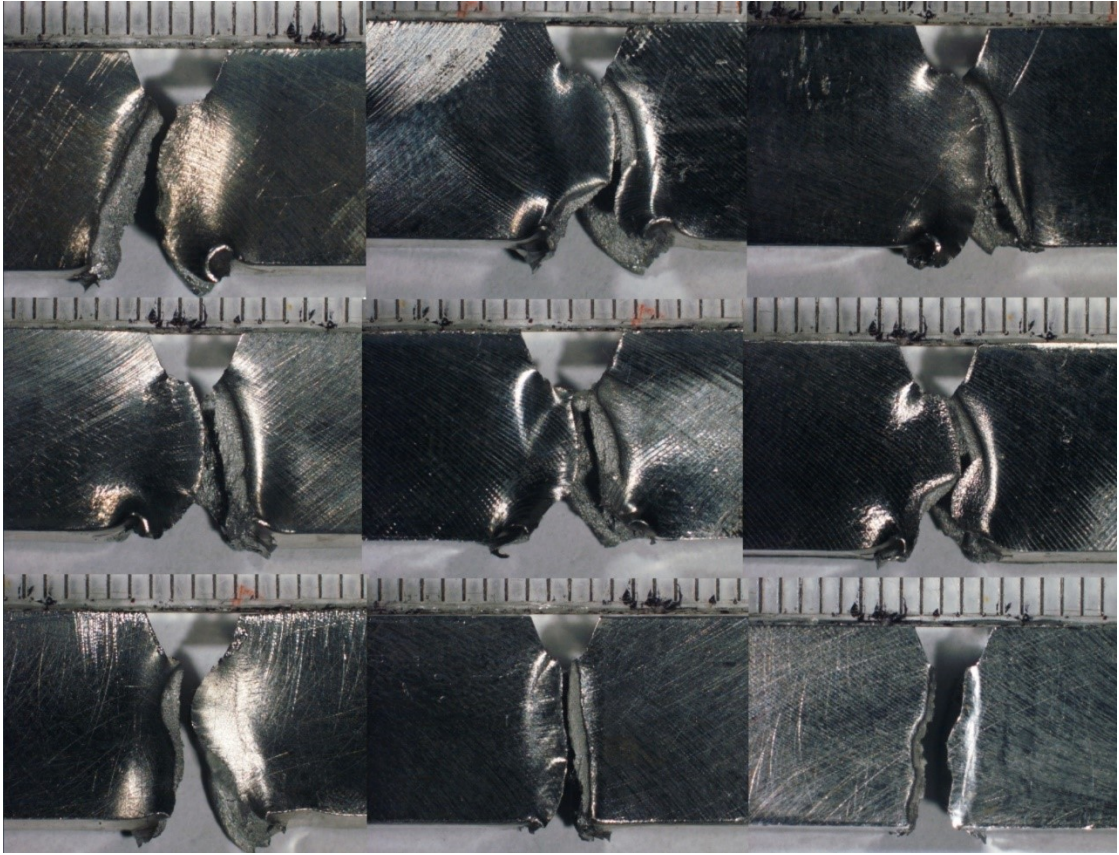
## Appendix 7 d)



*Fusion line\_max. Samples 10, 11, 12, 27, 28, 29, 44, 45 and 46.*

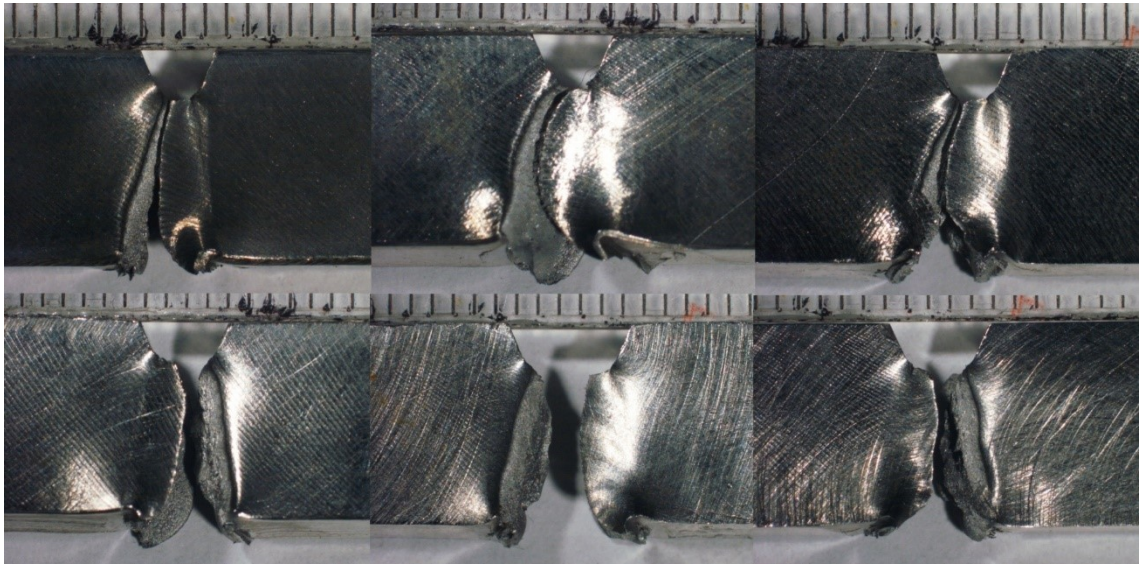


## Appendix 7 e)



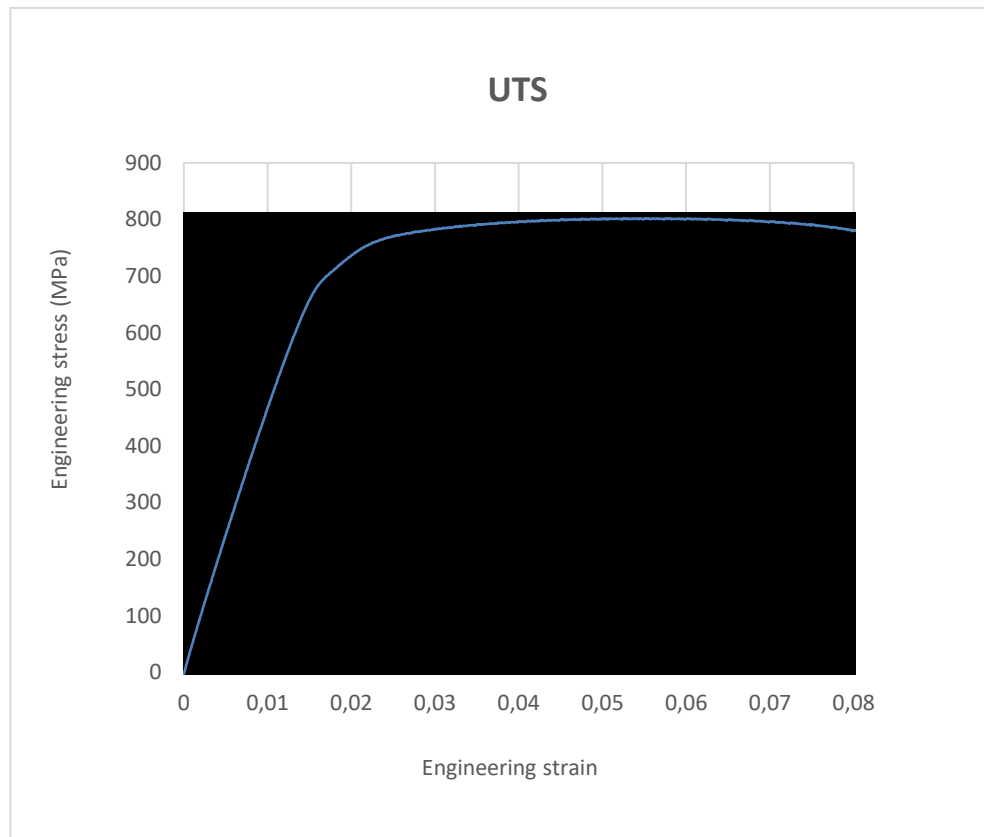
*Fusion line\_max +1 mm. Samples 15,16,17, 30, 31, 32, 47, 48 and 49.*

## Appendix 7 f)



*Fusion line\_max +3 and 5 mm. First three samples 16, 33, 50. Next three 17, 34 and 51.*

## Appendix 8



*Tensile test, stress-strain curve of welded S700MC sample.*



## Appendix 9



*Close-up picture of welded S700MC sample.*